Spin-isospin structure of the nuclear scissors mode

E. B. Balbutsev ⬤,[*] I. V. Molodtsova,[†] A. V. Sushkov,[‡] and N. Yu. Shirikova[¶]

Bogoliubov Laboratory of Theoretical Physics, Joint Institute for Nuclear Research, 141980 Dubna, Russia

P. Schuck

Institut de Physique Nucléaire, Centre National de la Recherche Scientifique IN2P3, Université Paris-Sud, F-91406 Orsay Cédex, France
and Université Grenoble Alpes, Centre National de la Recherche Scientifique, LPMMC, F-38000 Grenoble, France

The fine structure of the scissors mode is investigated within the time dependent Hartree-Fock-Bogoliubov (TDHFB) approach. The solution of TDHFB equations by the Wigner function moments (WFM) method predicts a splitting of the scissors mode into three intermingled branches. Together with the conventional scissors mode two new modes arise due to spin degrees of freedom. They generate significant $M1$ strength below the conventional energy range. The results of calculations of scissors resonances in rare earths and actinides by WFM and quasiparticle-phonon nuclear model methods are compared with experimental data. A remarkable coherence of both methods together with experimental data is observed.

I. INTRODUCTION

The idea of orbital nuclear scissors was reported by Hilton in 1976 at the International Conference on Nuclear Structure in Dubna [1] but the lecture remained unpublished. The first reasonable estimate of the energy of this collective excitation was given by Suzuki and Rowe [2]. However, they acknowledge discussions on the subject with Lo Iudice and Palumbo, whose ideas were published slightly later in [3]. The approach in this latter work was based on the so-called two rotor model (TRM) where the deformed proton distribution rotates against the neutron one in an oscillatory way, the restoring force being given by the symmetry energy of the liquid drop model. However, this model is presently not state of the art. As Lipparini and Stringari [4,5] and later Balbutsev *et al.* [6,7] have shown, microscopically there is a strong coupling between the scissors mode and the isovector giant quadrupole resonance. Actually without this coupling the scissors mode comes at zero energy (see [6,7]). Its first experimental detection in ^{156}Gd by the Darmstadt group [8] has initiated a cascade of experimental and theoretical studies. An exhaustive review of the subject is given in the paper [9] containing about 400 references.

The Wigner function moments (WFM) or phase space moments method [7,10] turned out to be very useful for the explanation of all qualitative features of the scissors mode. In the paper [11] the WFM method was generalized to solve the time dependent Hartree-Fock equations including spin

dynamics. The most remarkable result was the prediction of a new type of nuclear collective motion: rotational oscillations of "spin-up" nucleons with respect to "spin-down" nucleons (the spin scissors mode). A generalization of the WFM method which takes into account spin degrees of freedom and pair correlations simultaneously was outlined in [12], where the time dependent Hartree-Fock-Bogoliubov (TD-HFB) equations were considered. As a result the agreement between theory and experiment in the description of nuclear scissors modes was improved considerably. The evolution of our results in comparison with experimental data is shown in Fig. 1.

In principle, the scissors mode is believed to be a pure isovector mode. That is why we had divided the dynamical equations describing collective motion into isovector and isoscalar parts with the aim to separate the pure scissors mode. In the present paper, in order to study the interplay of isovector and isoscalar low-lying 1^+ excitations we solved the coupled dynamical equations of our model for protons and neutrons exactly, without the isovector-isoscalar decoupling. As a result one more magnetic mode (a third type of scissors) emerged (see Fig. 2 and explanations in Sec. III C). Actually, the possible existence of three scissors motions is easily explained by combinatoric consideration—there are only three ways to divide the four different kinds of objects (spin-up and spin-down protons and neutrons in our case) into two pairs. The analysis of the new situation, which appeared due to this last finding in the description of nuclear scissors, is presented in this paper.

The paper is organized as follows. In Sec. II the TDHFB equations for the 2×2 normal and anomalous density matrices are formulated and their Wigner transform is found, the model Hamiltonian is presented, collective variables are defined, and the respective dynamical equations are derived. In

───────

[*]balbuts@theor.jinr.ru
[†]molod@theor.jinr.ru
[‡]sushkov@theor.jinr.ru
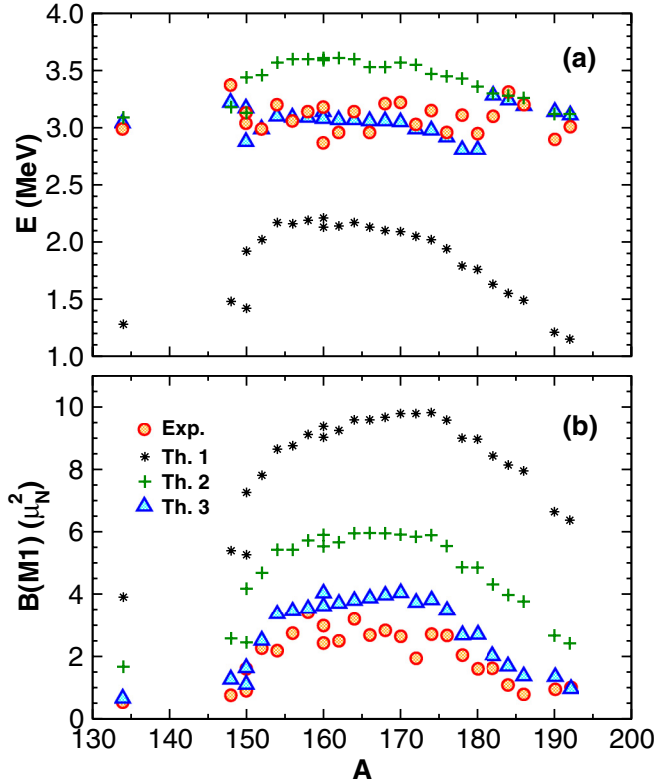[¶]shirikov@theor.jinr.ru

FIG. 1. Energy centroids E (a) and summed $B(M1)$ values (b) of the scissors mode. Th. 1, the results of calculations without spin degrees of freedom and pair correlations; Th. 2, pairing is included [13]; Th. 3, pairing and spin degrees of freedom are taken into account.

Sec. III the results of calculations of energies, $B(M1)$ values, and currents for nuclei of the $N = 82$–126 mass region and actinides are presented and discussed. In Sec. IV more elements for the understanding of the nature of the spin scissors modes are outlined. The summary of main results is given in the Conclusion section. The mathematical details can be found in Appendices A–C.

II. TDHFB EQUATIONS AND WFM EQUATIONS OF MOTION

The TDHFB equations in matrix formulation [14,15] are

$$i\hbar\dot{\mathcal{R}} = [\mathcal{H}, \mathcal{R}] \tag{1}$$

with

$$\mathcal{R} = \begin{pmatrix} \hat{\rho} & -\hat{\kappa} \\ -\hat{\kappa}^\dagger & 1 - \hat{\rho}^* \end{pmatrix}, \quad \mathcal{H} = \begin{pmatrix} \hat{h} & \hat{\Delta} \\ \hat{\Delta}^\dagger & -\hat{h}^* \end{pmatrix}. \tag{2}$$

The normal density matrix $\hat{\rho}$ and Hamiltonian $\hat{h}$ are hermitian whereas the anomalous density $\hat{\kappa}$ and the pairing gap $\hat{\Delta}$ are skew symmetric: $\hat{\kappa}^\dagger = -\hat{\kappa}^*$, $\hat{\Delta}^\dagger = -\hat{\Delta}^*$. The detailed form of the TDHFB equations is

$$i\hbar\dot{\hat{\rho}} = \hat{h}\hat{\rho} - \hat{\rho}\hat{h} - \hat{\Delta}\hat{\kappa}^\dagger + \hat{\kappa}\hat{\Delta}^\dagger,$$
$$-i\hbar\dot{\hat{\rho}}^* = \hat{h}^*\hat{\rho}^* - \hat{\rho}^*\hat{h}^* - \hat{\Delta}^\dagger\hat{\kappa} + \hat{\kappa}^\dagger\hat{\Delta},$$
$$-i\hbar\dot{\hat{\kappa}} = -\hat{h}\hat{\kappa} - \hat{\kappa}\hat{h}^* + \hat{\Delta} - \hat{\Delta}\hat{\rho}^* - \hat{\rho}\hat{\Delta},$$
$$-i\hbar\dot{\hat{\kappa}}^\dagger = \hat{h}^*\hat{\kappa}^\dagger + \hat{\kappa}^\dagger\hat{h} - \hat{\Delta}^\dagger + \hat{\Delta}^\dagger\hat{\rho} + \hat{\rho}^*\hat{\Delta}^\dagger. \tag{3}$$

Let us consider their matrix form in coordinate space keeping all spin indices s, s': $\langle \mathbf{r}, s|\hat{\rho}|\mathbf{r}', s'\rangle$, $\langle \mathbf{r}, s|\hat{\kappa}|\mathbf{r}', s'\rangle$, etc. We do not specify the isospin indices in order to make formulas more transparent. Let us introduce the more compact notation $\langle \mathbf{r}, s|\hat{X}|\mathbf{r}', s'\rangle = X_{rr'}^{ss'}$. Then the set of equations (3) with specified spin indices reads

$$i\hbar\dot{\rho}_{rr''}^{\uparrow\uparrow} = \int d^3r'(h_{rr'}^{\uparrow\uparrow}\rho_{r'r''}^{\uparrow\uparrow} - \rho_{rr'}^{\uparrow\uparrow}h_{r'r''}^{\uparrow\uparrow} + \hat{h}_{rr'}^{\uparrow\downarrow}\rho_{r'r''}^{\downarrow\uparrow} - \rho_{rr'}^{\uparrow\downarrow}h_{r'r''}^{\downarrow\uparrow} - \Delta_{rr'}^{\uparrow\downarrow}\kappa^{\dagger\downarrow\uparrow}_{r'r''} + \kappa_{rr'}^{\uparrow\downarrow}\Delta^{\dagger\downarrow\uparrow}_{r'r''}),$$

$$i\hbar\dot{\rho}_{rr''}^{\uparrow\downarrow} = \int d^3r'(h_{rr'}^{\uparrow\uparrow}\rho_{r'r''}^{\uparrow\downarrow} - \rho_{rr'}^{\uparrow\uparrow}h_{r'r''}^{\uparrow\downarrow} + \hat{h}_{rr'}^{\uparrow\downarrow}\rho_{r'r''}^{\downarrow\downarrow} - \rho_{rr'}^{\uparrow\downarrow}h_{r'r''}^{\downarrow\downarrow}),$$

$$i\hbar\dot{\rho}_{rr''}^{\downarrow\uparrow} = \int d^3r'(h_{rr'}^{\downarrow\uparrow}\rho_{r'r''}^{\uparrow\uparrow} - \rho_{rr'}^{\downarrow\uparrow}h_{r'r''}^{\uparrow\uparrow} + \hat{h}_{rr'}^{\downarrow\downarrow}\rho_{r'r''}^{\downarrow\uparrow} - \rho_{rr'}^{\downarrow\downarrow}h_{r'r''}^{\downarrow\uparrow}),$$

$$i\hbar\dot{\rho}_{rr''}^{\downarrow\downarrow} = \int d^3r'(h_{rr'}^{\downarrow\uparrow}\rho_{r'r''}^{\uparrow\downarrow} - \rho_{rr'}^{\downarrow\uparrow}h_{r'r''}^{\uparrow\downarrow} + \hat{h}_{rr'}^{\downarrow\downarrow}\rho_{r'r''}^{\downarrow\downarrow} - \rho_{rr'}^{\downarrow\downarrow}h_{r'r''}^{\downarrow\downarrow} - \Delta_{rr'}^{\downarrow\uparrow}\kappa^{\dagger\uparrow\downarrow}_{r'r''} + \kappa_{rr'}^{\downarrow\uparrow}\Delta^{\dagger\uparrow\downarrow}_{r'r''}),$$

$$i\hbar\dot{\kappa}_{rr''}^{\uparrow\downarrow} = -\hat{\Delta}_{rr''}^{\uparrow\downarrow} + \int d^3r'(h_{rr'}^{\uparrow\uparrow}\kappa_{r'r''}^{\uparrow\downarrow} + \kappa_{rr'}^{\uparrow\downarrow}h^{*\downarrow\downarrow}_{r'r''} + \Delta_{rr'}^{\uparrow\downarrow}\rho^{*\downarrow\downarrow}_{r'r''} + \rho_{rr'}^{\uparrow\uparrow}\Delta_{r'r''}^{\uparrow\downarrow}),$$

$$i\hbar\dot{\kappa}_{rr''}^{\downarrow\uparrow} = -\hat{\Delta}_{rr''}^{\downarrow\uparrow} + \int d^3r'(h_{rr'}^{\downarrow\downarrow}\kappa_{r'r''}^{\downarrow\uparrow} + \kappa_{rr'}^{\downarrow\uparrow}h^{*\uparrow\uparrow}_{r'r''} + \Delta_{rr'}^{\downarrow\uparrow}\rho^{*\uparrow\uparrow}_{r'r''} + \rho_{rr'}^{\downarrow\downarrow}\Delta_{r'r''}^{\downarrow\uparrow}). \tag{4}$$

This set of equations must be complemented by the complex conjugated equations. Writing these equations we neglected the diagonal in spin matrix elements of the anomalous density: $\kappa_{rr'}^{ss}$ and $\Delta_{rr'}^{ss}$. It was shown in [12] that such an approximation works very well in the case of monopole pairing considered here.

The microscopic Hamiltonian of the model, a harmonic oscillator with spin orbit potential plus separable quadrupole-quadrupole and spin-spin residual interactions, is given by

$$H = \sum_{i=1}^{A}\left[\frac{\hat{\mathbf{p}}_i^2}{2m} + \frac{1}{2}m\omega^2\mathbf{r}_i^2 - \eta\hat{\mathbf{l}}_i\hat{\mathbf{S}}_i\right] + H_{qq} + H_{ss}, \tag{5}$$
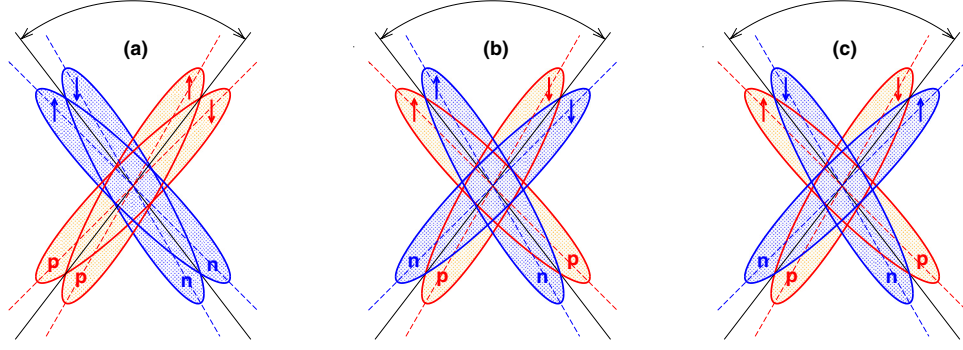
FIG. 2. Schematic representation of three possible types of scissors modes: (a) spin-scalar isovector (conventional, orbital scissors), (b) spin-vector isoscalar (spin scissors), and (c) spin-vector isovector (spin scissors). Arrows show the direction of spin projections: p, protons; n, neutrons. To avoid any possible misunderstanding it is necessary to emphasize that this is a schematic representation of the possible content of the three low lying solutions of the TDHFB equations for the density matrix which depends on spin and isospin projections and it should not be mixed up with the motions of four independent fluids. For a more quantitative representation see Sec. III C.

with

$$H_{qq} = \sum_{\mu=-2}^{2} (-1)^{\mu} \left\{ \bar{\kappa} \sum_{i}^{Z}\sum_{j}^{N} + \frac{\kappa}{2}\left[\sum_{i,j(i\neq j)}^{Z} + \sum_{i,j(i\neq j)}^{N} \right] \right\} q_{2-\mu}(\mathbf{r}_i)q_{2\mu}(\mathbf{r}_j), \tag{6}$$

$$H_{ss} = \sum_{\mu=-1}^{1} (-1)^{\mu} \left\{ \bar{\chi} \sum_{i}^{Z}\sum_{j}^{N} + \frac{\chi}{2}\left[\sum_{i,j(i\neq j)}^{Z} + \sum_{i,j(i\neq j)}^{N} \right] \right\} \hat{S}_{-\mu}(i)\hat{S}_{\mu}(j)\,\delta(\mathbf{r}_i - \mathbf{r}_j), \tag{7}$$

where $q_{2\mu} = \sqrt{16\pi/5}\, r^2 Y_{2\mu} = \sqrt{6}\{r \otimes r\}_{\lambda\mu}$, $\{r \otimes r\}_{\lambda\mu} = \sum_{\sigma,\nu} C_{1\sigma,1\nu}^{\lambda\mu} r_\sigma r_\nu$, $C_{1\sigma,1\nu}^{\lambda\mu}$ is the Clebsch-Gordan coefficient, cyclic coordinates r_{-1}, r_0, r_1 are defined in [16], and N and Z are the numbers of neutrons and protons. $\hat{S}_\mu$ are spin matrices [16]:

$$\hat{S}_1 = -\frac{\hbar}{\sqrt{2}}\begin{pmatrix} 0 & 1 \\ 0 & 0 \end{pmatrix}, \quad \hat{S}_0 = \frac{\hbar}{2}\begin{pmatrix} 1 & 0 \\ 0 & -1 \end{pmatrix}, \quad \hat{S}_{-1} = \frac{\hbar}{\sqrt{2}}\begin{pmatrix} 0 & 0 \\ 1 & 0 \end{pmatrix}. \tag{8}$$

Equations (4) will be solved by the WFM method in a small amplitude approximation. To this end we rewrite them with the help of the Wigner transformation [15]. So, instead of four matrix elements of the density matrix $\rho_{rr'}^{ss'}$ and two matrix elements $\kappa_{rr'}^{\uparrow\downarrow}$ and $\kappa_{rr'}^{\downarrow\uparrow}$ we will work with four Wigner functions $f^{ss'}(\mathbf{r},\mathbf{p})$ and two phase space distributions $\kappa^{ss'}(\mathbf{r},\mathbf{p})$, that is more convenient for WFM method (see [12,17] for details).

Integrating the transformed equations over phase space with the weights

$$W = \{r \otimes p\}_{\lambda\mu}, \{r \otimes r\}_{\lambda\mu}, \{p \otimes p\}_{\lambda\mu}, \text{ and } 1$$

one gets dynamic equations for the following collective variables:

$$\mathcal{L}_{\lambda\mu}^{\tau\varsigma}(t) = \int d(\mathbf{p},\mathbf{r})\{r \otimes p\}_{\lambda\mu}\delta f^{\tau\varsigma}(\mathbf{r},\mathbf{p},t),$$

$$\mathcal{R}_{\lambda\mu}^{\tau\varsigma}(t) = \int d(\mathbf{p},\mathbf{r})\{r \otimes r\}_{\lambda\mu}\delta f^{\tau\varsigma}(\mathbf{r},\mathbf{p},t),$$

$$\mathcal{P}_{\lambda\mu}^{\tau\varsigma}(t) = \int d(\mathbf{p},\mathbf{r})\{p \otimes p\}_{\lambda\mu}\delta f^{\tau\varsigma}(\mathbf{r},\mathbf{p},t),$$

$$\mathcal{F}^{\tau\varsigma}(t) = \int d(\mathbf{p},\mathbf{r})\delta f^{\tau\varsigma}(\mathbf{r},\mathbf{p},t),$$

$$\tilde{\mathcal{L}}_{\lambda\mu}^{\tau}(t) = \int d(\mathbf{p},\mathbf{r})\{r \otimes p\}_{\lambda\mu}\delta\kappa^{\tau i}(\mathbf{r},\mathbf{p},t),$$

$$\tilde{\mathcal{R}}_{\lambda\mu}^{\tau}(t) = \int d(\mathbf{p},\mathbf{r})\{r \otimes r\}_{\lambda\mu}\delta\kappa^{\tau i}(\mathbf{r},\mathbf{p},t),$$

$$\tilde{\mathcal{P}}_{\lambda\mu}^{\tau}(t) = \int d(\mathbf{p},\mathbf{r})\{p \otimes p\}_{\lambda\mu}\delta\kappa^{\tau i}(\mathbf{r},\mathbf{p},t), \tag{9}$$

where τ is the isospin index; $\varsigma = +, -, \uparrow\downarrow, \downarrow\uparrow$; and $\int d(\mathbf{p},\mathbf{r}) \equiv (2\pi\hbar)^{-3}\int d\mathbf{r}\int d\mathbf{p}$. δf and $\delta\kappa$ are variations of f and κ.

We are interested in the scissors mode with quantum number $K^\pi = 1^+$. Therefore, we only need the part of dynamic equations with $\mu = 1$. It is convenient to rewrite the dynamical equations for neutron and proton variables in terms of isoscalar and isovector variables $\mathcal{R}_{\lambda\mu} = \mathcal{R}_{\lambda\mu}^n + \mathcal{R}_{\lambda\mu}^p$, $\bar{\mathcal{R}}_{\lambda\mu} = \mathcal{R}_{\lambda\mu}^n - \mathcal{R}_{\lambda\mu}^p$, and so on. We also define isovector and isoscalar strength constants $\kappa_1 = \frac{1}{2}(\kappa - \bar{\kappa})$ and $\kappa_0 = \frac{1}{2}(\kappa + \bar{\kappa})$ connected by the relation $\kappa_1 = \alpha\kappa_0$ with $\alpha = -2$ [10]. The integration yields the sets of coupled equations for isovector and isoscalar variables which are written out in the Appendix A.

III. RESULTS OF CALCULATIONS

The calculations were performed for nuclei of the $N = 82$–126 mass region by the WFM method and in the frame of the quasiparticle-phonon nuclear model (QPNM). A short

TABLE I. The results of WFM calculations for ^{164}Dy: energies E (MeV), magnetic dipole $B(M1)$ (μ_N^2), and electric quadrupole $B(E2)$ (W.u.) strengths of 1^+ excitations. Isoscalar (IS) and isovector (IV) scenarios are valid only for the decoupled case. The excitations interpreted as scissors modes are marked in boldface.

	Decoupled equations			Coupled equations		
	E	$B(M1)$	$B(E2)$	E	$B(M1)$	$B(E2)$
IS	1.29	0.01	53.25	1.47	0.17	25.44
IV	**2.44**	**2.03**	0.34	**2.20**	**1.76**	3.30
IS	2.62	0.09	2.91	**2.87**	**2.24**	0.34
IV	**3.35**	**1.36**	1.62	**3.59**	**1.56**	4.37
IS	10.94	0.00	55.12	10.92	0.04	50.37
IS	14.04	0.00	2.78	13.10	0.00	2.85
IV	14.60	0.06	0.48	15.42	0.07	0.57
IS	15.88	0.00	0.55	15.55	0.00	1.12
IV	16.46	0.07	0.36	16.78	0.06	0.53
IS	17.69	0.00	0.45	17.69	0.01	0.68
IS	17.90	0.00	0.51	17.91	0.00	0.53
IV	18.22	0.18	1.85	18.22	0.13	0.89
IV	19.32	0.10	0.97	19.32	0.08	0.61
IV	21.29	2.47	31.38	21.26	2.03	21.60

outline of QPNM together with calculational details can be found in the papers [18,19]. Calculations for actinides will also be carried out by the WFM method. The procedure of calculations and parameters of the WFM method are mostly the same as in our previous paper [17].

A. $N = 82$–126 mass region

Let us analyze in detail the results of systematic calculations for nuclei of this mass region considering the example of Dy isotopes. The most interesting of them is ^{164}Dy, where a rather exceptional experimental situation with the low-lying 1^+ excitations exists. The results of the solution of Eqs. (A1) and (A2) for this nucleus are presented in Table I, where the energies of 1^+ levels with their magnetic dipole and electric quadrupole strengths (see Appendix B) are shown (left panel, the solutions of decoupled equations; right panel, isoscalar-isovector coupling taken into account). The first observation is that the high-lying levels are less sensitive to decoupling. Among the high-lying states $\mu = 1$ branches of isoscalar (at the energy of 10.92 MeV) and isovector ($E = 21.26$ MeV) giant quadrupole resonances are distinguished by large $B(E2)$ values. The rest of the high-lying states have quite small excitation probabilities and we omit them from further discussion.

The lowest level with an energy of 1.29 MeV is an isoscalar spin-scalar state of an irrotational nature with large $B(E2)$ value and practically zero $B(M1)$ strength. Taking into account the isoscalar-isovector coupling strongly affects this state, reducing its $B(E2)$ value by a factor of 2 (from 53 to 25 W.u.). However, it retains its electrical nature, and its energy changes only from 1.29 to 1.47 MeV (see Table I). The interpretation of this lowest electric level requires separate investigations. Its nature shall be studied in future work. Here we only note that this state inevitably appears in the theory and should be considered as part of the predictions.

Comparing the left and right panels, we see that the most remarkable change happens with the third low-lying level (an isoscalar one without coupling) acquiring a rather big magnetic strength with coupling. The "jump" from 0.09 μ_N^2 to 2.24 μ_N^2 looks surprising. However it is explained quite naturally by the structure of the matrix element of the excitation operator (see Appendix B). According to formula (B5) the contribution of isoscalar variables occurs with the factor $[g_s^n + g_s^p - g_l^p]$. Its numerical value (including the quenching factor $q = 0.7$) is 0.23. The contribution of isovector variables goes with the factors $\frac{1}{2}(g_s^p - g_s^n) = 3.29$ and $g_l^p = 1$, i.e., ≈ 20 times bigger than the isoscalar one. In the decoupled case the third level, being the isoscalar one, has the contribution only from isoscalar variables, which is obviously small. In the case with coupling it gets the additional contribution from isovector variables, which is an order of magnitude bigger. This explains the extraordinarily big increase of the $B(M1)$ value.

Thus, the coupling results in three magnetic levels of a mixed isovector-isoscalar nature. The three magnetic states correspond to three physically possible types of scissors modes already mentioned in the introduction. Roughly speaking the state at the energy 3.59 MeV in ^{164}Dy is predominantly the conventional "orbital" scissors mode, and the last two states at the energies 2.20 and 2.87 MeV are predominately the "spin" scissors modes. The detailed analysis of these three states is given in Sec. III C. Figure 2 shows a schematic representation of the possible content of these modes: the orbital scissors (neutrons versus protons) and two spin scissors (spin-up nucleons versus spin-down nucleons and a more complicated case—spin-up protons together with spin-down neutrons versus spin-down protons with spin-up neutrons). Both spin scissors exist only due to spin degrees of freedom.

So, the calculations without an artificial decoupling produce three low-lying magnetic states (instead of two without coupling). This is the main result of this paper.

In our example of ^{164}Dy the summarized magnetic strength $\sum B(M1) = 5.56$ μ_N^2 of three scissors is remarkably stronger than the analogous value $\sum B(M1) = 3.39$ μ_N^2 of two magnetic states in the case of decoupling (see Table I). One may say that it is also stronger than the respective experimental value. However, one must be careful here.

Trying to compare the theoretical results with the existing experimental data for the scissors mode, we encounter different summing interval conventions. It is assumed that the scissors mode includes only the states in a certain energy range. As a rule, the following two conventions are chosen, which lead to slightly different results for the summed $M1$ strength: $2.7 < E < 3.7$ MeV for $Z < 68$ and $2.4 < E < 3.7$ MeV for $Z \geqslant 68$ [20], and $2.5 < E < 4.0$ MeV for $82 \leqslant N \leqslant 126$ [21]. Only the two highest scissors fall into both of these intervals in ^{164}Dy (see Table I).

We have collected in Table II the experimental $B(M1)$ values found by nuclear resonance fluorescence (NRF) experiments for nuclei of the $N = 82$–126 mass region (see [20–22] and references therein). The last column of Table II contains the experimental $M1$ strength summed over the energy interval 1.8–4.0 MeV. We have also separated the 2.5–4.0-MeV range introduced as the area of orbital scissors [21] [see col-

TABLE II. The results of calculations by the WFM method and QPNM. In the case of WFM $i = 1$ means the lowest scissors and $i = 2$ means the centroid of two highest scissors; parameters are written out in Appendix A. The energy ranges for QPNM and NRF: 1.8–4.0 MeV ($i = 1$, 1.8–2.5 MeV; $i = 2$, 2.5–4.0 MeV).

Nuclei	δ	i	E_i (MeV)			$B_i(M1)$ (μ_N^2)			$\bar{E}$ (MeV)			$\sum B(M1)$ (μ_N^2)		
			WFM	QPNM	NRF	WFM	QPNM	NRF	WFM	QPNM	NRF	WFM	QPNM	NRF
^{148}Nd	0.17	1	2.51	2.47	2.38	0.28	0.41	0.09(02)	3.40	3.30	3.23	1.45	2.07	1.12(26)
		2	3.49	3.42	3.49	1.17	1.65	1.03(24)						
^{150}Nd	0.23	1	2.39	2.46		1.08	0.52		3.12	2.88	3.16	2.94	2.10	1.83(27)
		2	3.16	3.39	3.12	1.85	1.59	1.83(27)						
^{148}Sm	0.12	1	2.48	2.43		0.08	0.22		3.07	3.02	2.88	0.31	1.57	0.51(12)
		2	3.21	2.95	3.07	0.23	1.36	0.51(12)						
^{150}Sm	0.16	1	2.27			0.49			3.18	2.67	3.11	1.10	1.59	0.97(17)
		2	3.00	3.11	3.18	0.61	1.59	0.97(17)						
^{152}Sm	0.24	1	2.18	2.31		1.45	0.13		2.97	2.74	3.40	3.83	3.50[a]	2.41(33)
		2	3.08	3.21	2.97	2.38	2.51	2.41(33)						
^{154}Sm	0.26	1	2.22	2.19	2.23	1.59	0.83	0.33(12)	3.14	2.90	3.16	5.03	4.18	2.76(50)
		2	3.22	3.41	3.26	3.44	3.34	2.43(38)						
^{156}Gd	0.26	1	2.25	2.04	2.28	1.75	0.79	0.49(12)	2.94	2.87	3.02	5.06	4.92	3.22(68)
		2	3.19	3.20	3.06	3.31	4.13	2.73(56)						
^{158}Gd	0.26	1	2.22	2.34	2.37	1.70	0.48	0.28(06)	3.04	2.88	3.11	5.23	5.80	3.99(65)
		2	3.19	3.18	3.10	3.53	5.32	3.71(59)						
^{160}Gd	0.27	1	2.23	2.47	2.28	1.74	0.63	0.39(05)	3.10	2.97	3.08	5.96	5.82	4.41(54)
		2	3.27	3.15	3.17	4.22	5.18	4.02(49)						
^{160}Dy	0.26	1	2.25	2.43		1.84	1.07		2.87	2.84	3.05	5.19	5.14	2.42(30)
		2	3.17	3.22	2.87	3.35	4.07	2.42(30)						
^{162}Dy	0.26	1	2.22	2.46	2.40	1.80	1.40	0.52(03)	2.84	2.85	3.10	5.38	5.98	3.30(24)
		2	3.16	3.30	2.93	3.58	4.58	2.78(21)						
^{164}Dy	0.26	1	2.20	2.08		1.76	1.26		3.00	2.86	2.87	5.56	5.36	5.52(48)
		2	3.17	3.11	3.00	3.80	4.10	5.52(48)						
^{166}Er	0.26	1	2.23	2.04	1.95	1.89	1.35	0.58(10)	2.79	2.83	2.91	5.51	5.17	3.12(58)
		2	3.14	3.21	2.99	3.62	3.82	2.55(48)						
^{168}Er	0.26	1	2.20	2.32	2.49	1.81	1.14	0.17(02)	3.21	2.85	2.84	5.67	4.15	3.85(50)
		2	3.15	3.03	3.24	3.86	3.01	3.68(48)						
^{170}Er	0.26	1	2.18	2.14		1.81	1.45		3.22	2.85	3.01	5.87	5.20	2.63(39)
		2	3.15	3.35	3.22	4.06	3.75	2.63(39)						
^{172}Yb	0.25	1	2.18	2.16		1.86	0.53		2.93	2.74	3.04	5.26	4.06	2.37(49)
		2	3.05	3.17	2.93	3.40	3.53	2.37(49)						
^{174}Yb	0.25	1	2.16	2.10	2.18	1.82	0.86	0.63(33)	2.96	2.75	3.00	5.44	4.33	3.33(1.21)
		2	3.05	3.22	3.15	3.62	3.48	2.70(88)						
^{176}Yb	0.24	1	2.11	1.88	2.32	1.69	1.11	1.36(33)	2.86	2.69	2.91	5.02	4.47	3.24(1.05)
		2	2.99	3.25	3.25	3.33	3.36	1.88(72)						
^{176}Hf	0.23	1	2.66	2.21	2.04	1.08	1.04	0.13(01)	3.22	3.26	3.12	3.79	3.93	3.32(28)
		2	3.50	3.45	3.26	2.71	2.89	3.19(27)						
^{178}Hf	0.22	1	2.62	2.22		0.96	0.92		3.21	3.21	3.03	3.42	3.59	2.38(33)
		2	3.44	3.31	3.21	2.46	2.66	2.38(33)						
^{180}Hf	0.22	1	2.60	2.29	2.49	0.93	0.79	0.09(02)	3.16	3.22	3.14	3.51	3.66	2.13(30)
		2	3.44	3.37	3.19	2.58	2.86	2.04(28)						
^{182}W	0.20	1	2.59	2.29	2.47	0.80	0.01	0.31(05)	3.10	3.08	3.28	2.43	3.50	1.65(28)
		2	3.32	3.28	3.25	1.63	3.49	1.34(23)						
^{184}W	0.19	1	2.56	2.39	2.24	0.68	0.54	0.20(04)	3.19	3.02	3.29	2.05	3.49	1.24(37)
		2	3.35	3.45	3.37	1.37	2.96	1.04(33)						
^{186}W	0.18	1	2.53	2.40		0.57	0.01		3.19	2.96	3.40	1.68	3.27	0.82(21)
		2	3.18	3.40	3.19	1.11	3.25	0.82(21)						
^{190}Os	0.15	1	2.51		2.41	0.42		0.09(01)	2.83	3.01	3.37	2.09	1.93	0.94(12)
		2	3.13	3.37	2.87	1.68	1.93	0.85(11)						
^{192}Os	0.14	1	2.49			0.35			3.00	2.96	3.53	1.77	2.27	0.93(06)
		2	3.08	3.53	3.00	1.41	2.27	0.93(06)						

TABLE II. *(Continued.)*

Nuclei	δ	i	E_i (MeV)			$B_i(M1)$ (μ_N^2)			$\bar{E}$ (MeV)			$\sum B(M1)$ (μ_N^2)		
			WFM	QPNM	NRF	WFM	QPNM	NRF	WFM	QPNM	NRF	WFM	QPNM	NRF
^{194}Pt	0.12	1	2.50	2.23		0.32	0.06		3.25	2.91	3.48	1.32	1.06	1.31(23)
		2	3.05	3.56	3.25	1.00	1.00	1.31(23)						
^{196}Pt	0.11	1	2.47	2.27	2.25	0.26	0.02	0.06(02)	2.70	2.86	3.33	1.01	0.73	0.69(13)
		2	2.99	3.36	3.74	0.75	0.71	0.63(11)						

aThe level with energy $E = 4.14$ MeV was taken into account.

umn 9 (line $i = 2$)]. The $M1$ strength detected below 2.5 MeV is shown in the same column 9 ($i = 1$). The corresponding energy centroids are shown in columns 12 and 6. The WFM and QPNM calculation results are processed in the same way. In the case of WFM $i = 1$ means the lowest scissors and $i = 2$ means the centroid of the two highest scissors.

The $M1$ strength below 2.5 MeV was detected by the NRF only in 16 out of 28 nuclei considered in Table II. The $B(M1)$ of the lower group is always smaller than $B(M1)$ of the higher group. Comparing the values of the $B(M1)$ in columns 7 and 9, one can see that while there is a good agreement between theory and experiment for the higher energy region, for the lower one the theoretical values in most cases are several times larger than the observed ones. This may be partly due to the difficulty of NRF experiments in separating weaker transitions from the atomic background in the low energy range [23]. If, with more careful measurements, the additional $M1$ strength turns out to be negligible, one will have to conclude that the NRF data do not support the theory in this part.

Generally speaking, such a division of the spectrum into regions is rather artificial. It was introduced in an attempt to separate the purely orbital scissors mode. Our results demonstrate that the contribution of the spin to the formation of the scissors resonance (SR) is very significant. Accounting for spin degrees of freedom and isovector-isoscalar coupling generates spin scissors modes and splits the resonance into three branches. In addition, as will be shown below, taking into account the spin part of the magnetic dipole operator significantly affects the $B(M1)$ value of all scissors states. In this regard, we think that it is more reasonable to compare the WFM results with the summed $M1$ strength in the entire region of 1.8–4.0 MeV.

We also believe that some portion of the spin contribution associated with spin scissors may have been missed in the NRF experiments. So, for all these reasons, we first compare WFM results for the energy centroids $E_{i=2}$ (column 4 in Table II) and summed $B_{i=2}(M1)$ values (column 7) of only the two highest scissors mode with NRF centroids and summed $B(M1)$ (columns 12 and 15, respectively). This comparison is displayed also in Fig. 3 (the theory results are marked as WFM1). It turns out that with this selection, the overall agreement between the theoretical and experimental results is very good—there are only three (out of 28) remarkable differences for $B(M1)$ values (^{160}Dy, ^{170}Er, and ^{172}Yb) and three ones for energies (^{160,162}Dy and ^{166}Er). The energy centroids and summed $B(M1)$ values of all three scissors are shown in columns 10 and 13 in Table II. These data are also shown in Fig. 3 (WFM2). Only for ^{164}Dy there is the excellent

agreement of the theory and experiment. In the remaining nuclei an equally significant low energy $M1$ strength was not detected in the NRF experiments. However, WFM calculations predict the existence of comparable magnetic strength in all well-deformed nuclei of this mass region. This prediction is supported by calculations in the frame of the QPNM (see Table II and Fig. 4).

The situation with the lowest scissors is very interesting. It helps to explain the experimentally observed features of the 1^+ spectrum of ^{164}Dy. Figure 5 demonstrates experimental $M1$ strength distributions in ^{160,162,164}Dy in the energy range between 2 and 4 MeV, reported by Margraf *et al.* [24]. Obviously, there are two groups of strong $M1$ excitations in ^{164}Dy around 2.6 and 3.1 MeV. However, only the upper group was attributed to the scissors mode, and the group around 2.6 MeV was not included because it has a rather big spin contribution and one level has pure two-quasiparticle nature and the summed $M1$ strength of both groups strongly deviates from the scissors mode systematics in the rare-earth nuclei [21]. The results of WFM calculations allow one to clarify the origin of both groups. Table III demonstrates that the energy centroid and summed $B(M1)$ value of the observed lower group agree very well with the calculated energy E and $B(M1)$ value of the lowest scissors. The respective values of the observed higher group are in excellent agreement with
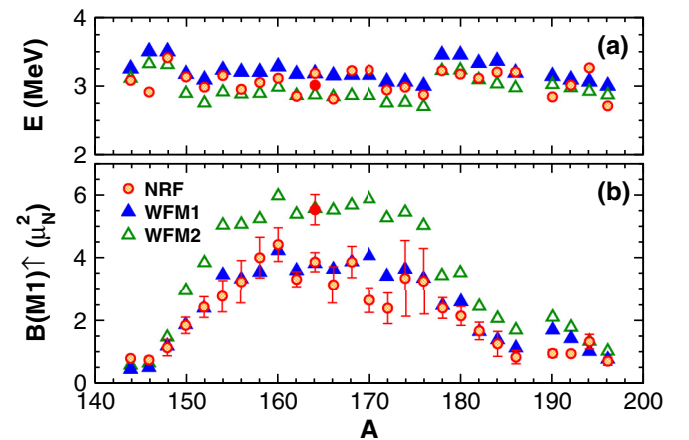

FIG. 3. Calculated (WFM) and experimental (NRF) mean excitation energies (a) and summed $M1$ strengths (b) of the scissors mode. WFM1, the sum of the two highest scissors; WFM2, the sum of three scissors. Experimental data are taken from the papers listed in Table I of [21]. The solid circle marks the experimental result for ^{164}Dy when summed in the energy range 1.8−4.0 MeV.
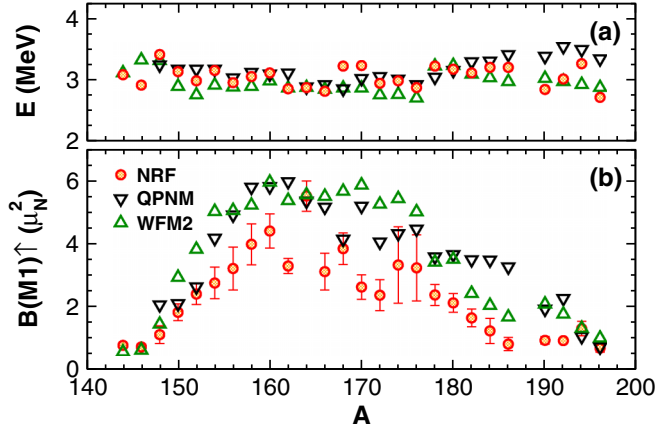
FIG. 4. WFM2, energy centroid of three scissors and the respective $B(M1)$ value given by WFM method; QPNM, analogous values calculated in the frame of QPNM in the energy range 1.8–4.0 MeV; and NRF, experimental data.

the calculated energy centroid and summed $B(M1)$ of the two remaining (higher in energy) scissors.

The calculations with and without the spin part of the dipole magnetic operator (B4) show that all three scissors states are equally sensitive to the spin dependent part of the external field (compare columns 2 and 3 in Table III) in agreement with analogous findings of other authors (see for example [25,26]). The enhancement of the spin contribution to $B(M1)$ plays in favor of spin scissors.

So, according to our results, the low energy group of states in ^{164}Dy is also a branch of the scissors mode (spin-vector isovector scissors) and the calculated summed magnetic strength 5.56 μ_N^2 is in excellent agreement with the experimental value 5.52 μ_N^2 (sum of both groups). Analogous values for two other Dy isotopes, ^{160}Dy and ^{162}Dy, are predicted to
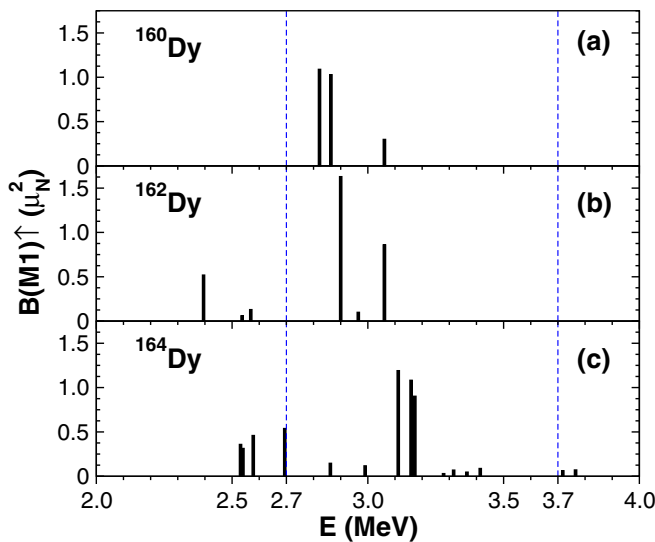
FIG. 5. Excitation energies E with the corresponding $B(M1)$ values, obtained by the NRF experiment [24]. The dashed lines mark the boundaries of the conventional interval from [20].

TABLE III. The calculated energies E (MeV) and excitation probabilities $B(M1)$ (μ_N^2) of three scissors are compared with experimental values $\bar{E}$ and $\sum B(M1)$ of two groups of 1^+ levels in ^{164}Dy [24]. q, spin quenching factor; $g_s^\tau = q g_s^{\tau\,\text{free}}$; $q = 0$ means that the spin part of the external field (B4) is omitted.

	Theory (WFM)				Experiment (NRF)	
	$B(M1)$					
E	$q = 0$	$q = 0.7$	$\bar{E}$	$\sum B(M1)$	$\bar{E}$	$\sum B(M1)$
2.20	0.53	1.76	2.20	1.76	2.60	1.67(14)
2.87	1.52	2.24				
3.59	6.63	1.56	3.17	3.80	3.17	3.85(31)

be 5.19 μ_N^2 and 5.38 μ_N^2 (see Table IV). This result is supported by the QPNM calculations, which also demonstrates for ^{160,162,164}Dy isotopes remarkable $M1$ strength below the conventional energy interval.

From a glance at Fig. 5 it becomes clear that the situation in ^{160,162}Dy observed by NRF experiments is quite different from that of ^{164}Dy. However, our prediction may be in accord with the recent results of photoneutron measurements performed by the Oslo group. In [23] the authors revised their previous data on the SR in $^{160-164}$Dy obtained by the Oslo method. The essence of their findings is formulated in the following quotation from [23]: "The present fit strategy gives about 40% higher summed SR strengths than the reported NRF results. However, if we apply the NRF energy limits to Eq. (19), we obtain excellent agreement with the NRF results.... It is interesting to note that $\approx$40–60% of our measured SR strength lies in the energy region below 2.7 MeV."

Though the statements about "40% higher" and "$\approx$40–60% ... below 2.7 MeV" could be in qualitative or even semiquantitative agreement with our results, unfortunately, the error bars of the Oslo data are much too large to be considered much more than an eventual "smoking gun." So, we cannot use the Oslo results for a undoubted support of our findings. Only more precise data can clear up the situation from the experimental point of view.

The energy centroids and corresponding summed $B(M1)$ given by the WFM theory and by the QPNM calculations for Dy isotopes are compared with experimental results from the NRF and from photoneutron measurements (Oslo) [23] in Table IV. The results are shown for various energy averaging intervals. As it is seen, the theoretical results are in very good overall agreement for all three Dy isotopes. It is worthwhile to note the excellent agreement between all theoretical and experimental results for ^{164}Dy. In Fig. 6 the summed $B(M1)$ values are also shown for ^{160,162,164}Dy including this time the results from Gogny quasiparticle random phase approximation (QRPA) calculations and the experimental results obtained by the photoneutron measurements (Oslo) [23] and radiative capture of resonance neutrons [27]. It is noteworthy that the WFM results are in good agreement both with two other more complex theoretical results and with the available experimental data. We tend to view this as a support of our assumption that in fact not one but three intermingled scis-

TABLE IV. The energy centroids $\bar{E}$ and corresponding summed $B(M1)$ values given by WFM and QPNM are compared with experimental results by the NRF [24] and photoneutron measurements (Oslo) [23] for ^{160,162,164}Dy. Comparison is presented for various energy intervals.

	Theory				Experiment			
	WFM		QPNM		NRF		Oslo	
^{A}Dy	$\bar{E}$ (MeV)	$B(M1)$ (μ_N^2)	$\bar{E}$ (MeV)	$B(M1)$ (μ_N^2)	$\bar{E}$ (MeV)	$B(M1)$ (μ_N^2)	$\bar{E}$ (MeV)	$B(M1)$ (μ_N^2)
	$2.7 < E < 3.7$ MeV				$2.7 < E < 3.7$ MeV			
^{160}Dy	3.17	3.35	3.05	3.17	2.87	2.42(30)	2.66(12)	1.7(10)
^{162}Dy	3.16	3.58	3.08	3.27	2.96	2.59(19)	2.81(8)	2.3(8)
^{164}Dy	3.17	3.80	3.26	2.13	3.17	3.85(31)	2.83(8)	2.8(9)
	$2.0 < E < 4.0$ MeV				$2.0 < E < 4.0$ MeV		$0 < E < 10$ MeV	
^{160}Dy	2.84	5.19	3.05	5.14	2.87	2.42(30)	2.66(12)	4.8(26)
^{162}Dy	2.85	5.38	3.10	5.98	2.84	3.30(24)	2.81(8)	4.8(17)
^{164}Dy	2.86	5.56	2.87	5.36	3.00	5.52(48)	2.83(8)	5.5(18)

sors modes are involved: the conventional one and two spin scissors which may be to a good proportion isovector spin vector and isoscalar spin vector in nature. As mentioned, this is just the natural triplet of scissors modes which one obtains from pure combinatorics. The detailed spin-isospin balance between the three modes will be discussed in Sec. III C.

B. Actinides

The scissors mode is especially pronounced in stable nuclei with significant deformation, such as rare-earth nuclei and in the region of actinides. Low-lying $M1$ strength has been observed in several actinide nuclei. Experimental studies of
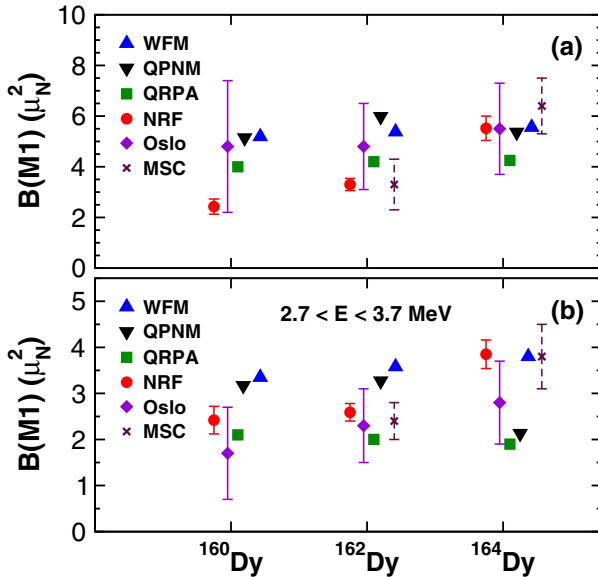

FIG. 6. Comparison of the summed $B(M1)$ values for SR in ^{160,162,164}Dy from the present WFM theory, the QPNM and Gogny QRPA [23] calculations with the experimental values from the NRF [24], photoneutron measurements (Oslo) [23] (with very large error bars), and multistep-cascade (MSC) measurements of γ decay following neutron capture [27]. (a) Averaging energy intervals are 2–4 MeV for WFM, QPNM, and NRF; 0–3.5 MeV for QRPA; and 0–10 MeV for Oslo and MSC. (b) The averaging interval is 2.7–3.7 MeV.
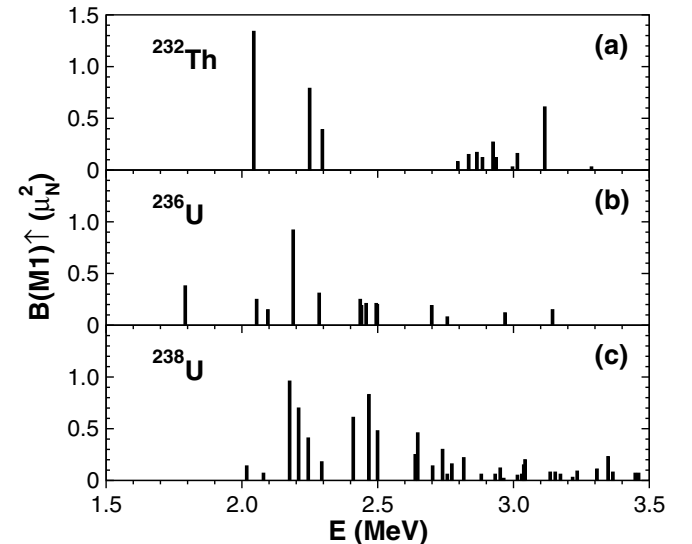
scissors mode excitation by nuclear resonance fluorescence in the actinides have been reported for ^{232}Th [28,29], ^{236}U [30], and ^{238}U [29,31]. The experimental and theoretical situation for ^{232}Th, ^{236}U, and ^{238}U has been carefully analyzed in [31]. Studies of the scissors resonance excited by deuteron and ^{3}He-induced reactions on ^{232}Th in residual nuclei ^{231,232,233}Th and ^{232,233}Pa using the Oslo method have also been reported in [32]. It was found that the scissors mode spectrum of many of the nuclei studied exhibits a distinct double-humped structure (see [28,32] and discussion in [17]). The experimentally observed spectra of 1^+ excitations in ^{232}Th [28], ^{236}U [30], and ^{238}U [31] are shown in Fig. 7. The data show a clear splitting of the scissors resonance strength in ^{232}Th.

In our calculations, the case of actinides is similar to the rare-earth region (see Table V and Fig. 8). The scissors resonance is split into three branches. Since the SR roughly follows the inverse mass dependence of $\sim A^{-1/3}$, the spectrum in actinides is shifted towards lower energies. In all the nuclei studied, ^{232}Th and ^{236,238}U, the lowest state is localized at

FIG. 7. The experimentally observed spectra of 1^+ excitations in (a) ^{232}Th [28], (b) ^{236}U [30], and (c) ^{238}U [31].

TABLE V. The nuclear scissors mode fine structure. The results of calculations by the WFM method: energies E_i with corresponding $B_i(M1)$ values. Energy centroids $\bar{E}$ and summed $M1$ strengths are also presented. Parameters of pair correlations: $V_0^p = 25.5$ MeV, $V_0^n = 21.5$ MeV, $r_p^p = 1.5$ fm, $r_p^n = 1.80$ fm; $\kappa_{\text{Nils}} = 0.06$, $q = 0.7$.

Nuclei	δ	i	E_i (MeV)	$B_i(M1)$ (μ_N^2)	$\bar{E}_{[2-3]}$ (MeV)		$\sum_{i=2}^{3} B_i(M1)$ (μ_N^2)		$\bar{E}_{[1-3]}$ (MeV)	$\sum_{i=1}^{3} B_i(M1)$ (μ_N^2)
			WFM		WFM	NRF	WFM	NRF	WFM	WFM
^{232}Th	0.216	1	1.53	1.70						
		2	2.21	2.55	2.43	2.49	4.07	4.26(64)	2.16	5.77
		3	2.81	1.51						
^{236}U	0.220	1	1.54	1.91						
		2	2.22	2.87	2.44	2.35	4.51	4.06(61)	2.17	6.41
		3	2.82	1.64						
^{238}U	0.234	1	1.57	2.12						
		2	2.32	3.69	2.54	2.58	5.80	7.59(1.2)	2.28	7.92
		3	2.93	2.10						

the energy of about 1.55 MeV, while in the rare earths it is 2.2–2.6 MeV. The calculated energy centroids and summed $B(M1)$ values of the two highest scissors in ^{232}Th are in excellent agreement with experimental NRF data. The agreement between the analogous values in ^{236}U can be characterized as acceptable.

In addition, Fig. 8 demonstrates that the average energy and the summed magnetic strength of the lower group of levels in ^{232}Th practically exactly coincide with the energy and $B(M1)$ value of the middle ($E = 2.21$ MeV) calculated scissors mode and the analogous values of the higher group of levels are in very good agreement with the energy and $B(M1)$ value of the highest ($E = 2.81$ MeV) scissors mode given by the theory. A similar picture can be obtained for ^{236}U if to divide its spectrum in two groups, the boundary between them being chosen in the energy window $2.3 < E < 2.4$ MeV (see Fig. 7).

One observes an unexpectedly large value of the summed $B(M1)$ for ^{238}U in comparison with that of ^{236}U and ^{232}Th and with the theoretical result for the energy region above 2.0 MeV. The possible reason for this discrepancy was indicated by the authors of [31]: "$M1$ excitations are observed

FIG. 8. The centroids of experimentally observed spectra of 1^+ excitations in ^{232}Th (a) and ^{236}U (b) (black rectangles with error bars) are compared with the results of WFM calculations (red rectangles).

at approximately 2.0 MeV $< E_\gamma < 3.5$ MeV with a strong concentration of $M1$ states around 2.5 MeV. . … The observed $M1$ strength may include states from both the scissors mode and the spin-flip mode, which are indistinguishable from each other based exclusively on the use of the NRF technique." The most reasonable (and quite natural) place for the boundary between the scissors mode and the spin-flip resonance is located in the spectrum gap between 2.5 and 2.62 MeV (see Fig. 7). The summed $M1$ strength of scissors in this case becomes $B(M1) = 4.38 \pm 0.5$ μ_N^2 in rather good agreement with ^{236}U and ^{232}Th. However, one cannot be satisfied by this agreement, because this value turns out a little bit too small in comparison with the theoretical result 5.8 μ_N^2. In addition, having remarkably bigger deformation, ^{238}U is expected to have bigger $M1$ strength than ^{236}U and ^{232}Th according to the experimentally established rule $B(M1) \sim \delta^2$. In this connection it makes sense to consider another possible place for the required boundary. If one puts it into the less pronounced spectrum gap between 2.82 and 2.88 MeV, then the summed $B(M1)$ of scissors becomes 5.97 μ_N^2 which agrees rather well with the theoretical value. However, more studies should be undertaken to definitely clear up the situation.

Note also that the $B(M1)$ value calculated within QPNM in the energy range 2.1–2.5 MeV is equal to 3.3 μ_N^2 [33]. As can be seen from Table V, in that energy region the proper state given by WFM theory is located at $E = 2.32$ MeV with $B(M1) = 3.69$ μ_N^2.

Comparison of the results presented in this paper with those obtained earlier without taking into account the isovector-isoscalar coupling shows that the overall picture remains practically unchanged, if the lowest state at 1.55 MeV is left out. The agreement with experiment for the summarized $M1$ strength over two states became even slightly better (compare Table V and Fig. 8 with Table II and Fig. 8 in [17]). Thus, for example, the $B(M1) = 4.07$ μ_N^2 for ^{232}Th is closer to the experimental value of 4.26(64) μ_N^2 than the 3.82 μ_N^2 reported in [17]. The presence of an additional magnetic dipole strength around 1.5 MeV should be considered as a prediction.
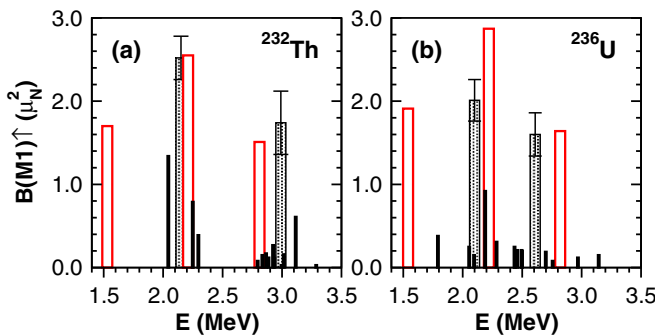
In this regard, it is worth noting an interesting detail of the ^{236}U spectrum. Its lowest level is disposed remarkably lower than 2 MeV and is separated by a remarkable energy gap from the higher levels. This makes it possible to interpret this level as a small fraction of the lowest scissors predicted by the theory. A possible involvement of the spin flip cannot be ruled out either (see the discussion in Sec. IV C).

Again for ^{238}U it is noteworthy that the summed $B(M1)$ value, equal to 7.92 μ_N^2 (see Table V), is in good agreement with both the results of QPNM calculations of 7.02 μ_N^2 [19,33], obtained by summation in the energy range from 1 to 3 MeV, and the observed $M1$ strength 7.59(1.2) μ_N^2 [31].

Summarizing the results presented in these two sections, we can conclude that, in general, there is good agreement between both theories and experimental data. Concerning the lowest magnetic states in the rare earths and in the actinides we can repeat that it is a prediction.

C. Currents

When studying little collective states where shell effects are dominated, it is not easy to extract from the quantal QRPA results a global average trend. However, the macroscopic WFM approach does just this. It only yields the average trends. This kind of features has already become manifest for the study of moments of inertias of superfluid nuclei. The microscopic picture of the corresponding flows is quite erratic due to the strong shell effects (see [34]), while a semiclassical calculation very nicely shows a mixture of rigid and irrotational flows which very well accounts for the experimental situation on average (see [34,35]). We think with more data to come we will see the same situation emerging for spin scissors currents and $B(M1)$.

Figure 2 gives a schematic view of all possible nuclear scissors motions. To obtain an objective picture of the phenomenon it is necessary to study the distribution of neutron and proton currents $J_i^\varsigma(\mathbf{r})$. By definition the current is obtained by the odd in $\mathbf{p}$ part of the phase space distribution:

$$J_i^\varsigma(\mathbf{r}, t) = \int \frac{d\mathbf{p}}{(2\pi\hbar)^3} p_i f^\varsigma(\mathbf{r}, \mathbf{p}, t). \tag{10}$$

An isospin index is omitted for simplicity. In [10], where the simple model of a harmonic oscillator with separable qq interaction was considered, the analytical formula for the nucleons' flows was derived. In the case with spin degrees of freedom and pair correlations the currents can be constructed only numerically. According to the approximation suggested in [36,37] the current variation is expanded in the following series:

$$\delta J_i^\varsigma(\mathbf{r}, t) = n^+(\mathbf{r})\Bigg[K_i^\varsigma(t) + \sum_j (-1)^j K_{i,-j}^\varsigma(t) r_j$$
$$+ \sum_{\lambda',\mu'} (-1)^{\mu'} K_{i,\lambda'-\mu'}^\varsigma(t)\{r \otimes r\}_{\lambda'\mu'} + \cdots \Bigg]. \tag{11}$$

All terms containing expansion coefficients K with odd numbers of indices disappear due to axial symmetry. Furthermore, we truncate this series omitting all terms generating higher than second order moments. So, finally the following expression is used:

$$\delta J_i^\varsigma(\mathbf{r}, t) = n^+(\mathbf{r}) \sum_j (-1)^j K_{i,-j}^\varsigma(t) r_j. \tag{12}$$

The detailed expressions are

$$\delta J_1^\varsigma = n^+\big(K_{1,0}^\varsigma r_0 - K_{1,-1}^\varsigma r_1 - K_{1,1}^\varsigma r_{-1}\big),$$
$$\delta J_0^\varsigma = n^+\big(K_{0,0}^\varsigma r_0 - K_{0,-1}^\varsigma r_1 - K_{0,1}^\varsigma r_{-1}\big),$$
$$\delta J_{-1}^\varsigma = n^+\big(K_{-1,0}^\varsigma r_0 - K_{-1,-1}^\varsigma r_1 - K_{-1,1}^\varsigma r_{-1}\big).$$

The coefficients $K_{i,-j}^\varsigma(t)$ are connected by linear relations with the collective variables $\mathcal{L}_{\lambda\mu}^\varsigma(t)$ (see Appendix C). Taking into account that in the frame of the problem considered here $\mathcal{L}_{\lambda0}^\varsigma = \mathcal{L}_{\lambda2}^\varsigma = 0$, we find for $\varsigma = +, -$

$$\delta J_1^\varsigma = n^+\alpha_1\big(\mathcal{L}_{21}^\varsigma - \mathcal{L}_{11}^\varsigma\big)r_0,$$
$$\delta J_0^\varsigma = n^+\alpha_2\big[\big(\mathcal{L}_{2-1}^\varsigma - \mathcal{L}_{1-1}^\varsigma\big)r_1 + \big(\mathcal{L}_{21}^\varsigma + \mathcal{L}_{11}^\varsigma\big)r_{-1}\big],$$
$$\delta J_{-1}^\varsigma = n^+\alpha_1\big(\mathcal{L}_{2-1}^\varsigma + \mathcal{L}_{1-1}^\varsigma\big)r_0,$$

where $\alpha_i = \sqrt{3}/(\sqrt{2}A_i)$ and A_i are defined by (A3). The expressions for currents in Cartesian coordinates are written

$$\delta J_x^\varsigma = \big(\delta J_{-1}^\varsigma - \delta J_1^\varsigma\big)/\sqrt{2}$$
$$= \frac{1}{\sqrt{2}} n^+\alpha_1\big(\mathcal{L}_{2-1}^\varsigma - \mathcal{L}_{21}^\varsigma + \mathcal{L}_{1-1}^\varsigma + \mathcal{L}_{11}^\varsigma\big)z,$$
$$\delta J_y^\varsigma = i\big(\delta J_{-1}^\varsigma + \delta J_1^\varsigma\big)/\sqrt{2}$$
$$= \frac{i}{\sqrt{2}} n^+\alpha_1\big(\mathcal{L}_{2-1}^\varsigma + \mathcal{L}_{21}^\varsigma + \mathcal{L}_{1-1}^\varsigma - \mathcal{L}_{11}^\varsigma\big)z,$$
$$\delta J_z^\varsigma = \delta J_0^\varsigma = n^+\alpha_2\big[\big(\mathcal{L}_{21}^\varsigma - \mathcal{L}_{2-1}^\varsigma + \mathcal{L}_{11}^\varsigma + \mathcal{L}_{1-1}^\varsigma\big)x$$
$$- \frac{i}{\sqrt{2}}\big(\mathcal{L}_{21}^\varsigma + \mathcal{L}_{2-1}^\varsigma + \mathcal{L}_{11}^\varsigma - \mathcal{L}_{1-1}^\varsigma\big)y\big]. \tag{13}$$

According to their definition $\mathcal{L}_{2-1}^\varsigma = \mathcal{L}_{21}^\varsigma$ and $\mathcal{L}_{1-1}^\varsigma = -\mathcal{L}_{11}^\varsigma$ (with $\varsigma = +, -$). Therefore we have

$$\delta J_x^\varsigma = 0,$$
$$\delta J_y^\varsigma = -i\frac{\sqrt{3}}{A_1} n^+\big(\mathcal{L}_{11}^\varsigma - \mathcal{L}_{21}^\varsigma\big)z,$$
$$\delta J_z^\varsigma = -i\frac{\sqrt{3}}{A_2} n^+\big(\mathcal{L}_{11}^\varsigma + \mathcal{L}_{21}^\varsigma\big)y. \tag{14}$$

This result is quite remarkable. The first equation $\delta J_x^\varsigma = 0$ says that all motions take place only in two dimensions, i.e., in one plane. Obviously it is one of the properties to be satisfied by the scissors mode. Another obvious and necessary property of the scissors mode is the rotational out of phase motion of its subentities. This property is demonstrated by the pictures of currents (see Figs. 9–11) constructed with the help of Eqs. (14).

Let us analyze these figures. First of all it is seen that one cannot identify any of three $M1$ excitations with only one type of motions shown in Fig. 2—it turns out that every excitation is a mixture of all three possible scissors. Nevertheless an approximate identification can be done. It is necessary to introduce some numerical measure of the contribution of every type of scissors into the particular excitation. Introducing the
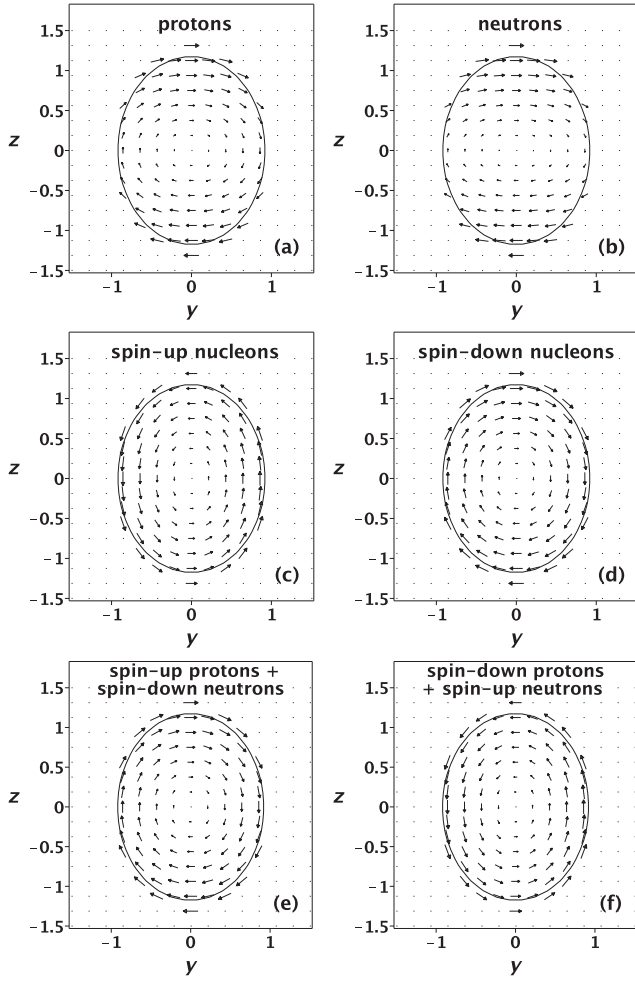
FIG. 9. The currents in ^{164}Dy for $E = 2.20$ MeV: δJ_p^+ (a), δJ_n^+ (b), $\delta J^{\uparrow\uparrow}$ (c), $\delta J^{\downarrow\downarrow}$ (d), $\delta J_p^{\uparrow\uparrow} + \delta J_n^{\downarrow\downarrow}$ (e), and $\delta J_p^{\downarrow\downarrow} + \delta J_n^{\uparrow\uparrow}$ (f). $\mathsf{y} = y/R$, $\mathsf{z} = z/R$.

FIG. 10. The currents in ^{164}Dy for $E = 2.87$ MeV: δJ_p^+ (a), δJ_n^+ (b), $\delta J^{\uparrow\uparrow}$ (c), $\delta J^{\downarrow\downarrow}$ (d), $\delta J_p^{\uparrow\uparrow} + \delta J_n^{\downarrow\downarrow}$ (e), and $\delta J_p^{\downarrow\downarrow} + \delta J_n^{\uparrow\uparrow}$ (f). $\mathsf{y} = y/R$, $\mathsf{z} = z/R$.

notations [see Eqs. (14)]

$$A^\varsigma = -i\frac{\sqrt{3}}{A_2}(\mathcal{L}_{11}^\varsigma + \mathcal{L}_{21}^\varsigma),$$

$$B^\varsigma = -i\frac{\sqrt{3}}{A_1}(\mathcal{L}_{11}^\varsigma - \mathcal{L}_{21}^\varsigma),$$

we can construct the following indicator characterizing the definite scissors, for example, the conventional one:

$$AB_{(ab)} = [A^2 + B^2]_{(a)} + [A^2 + B^2]_{(b)}.$$

Analogous values $AB_{(cd)}$ and $AB_{(ef)}$ are defined also for spin scissors. After normalization all three values are transformed in percents, which are shown in Table VI together with the respective values of A and B. The simple analysis of this table allows one to conclude the following.

(1) Excitation with $E = 2.20$ MeV represents predominantly (51%) the "complicated" spin scissors [Figs. 9(e) and 9(f)] with rather strong admixture (47%) of the "simple" spin scissors [Figs. 9(c) and 9(d)].

(2) Excitation with $E = 2.87$ MeV represents predominantly (54%) the simple spin scissors [Figs. 10(c) and 10(d)]
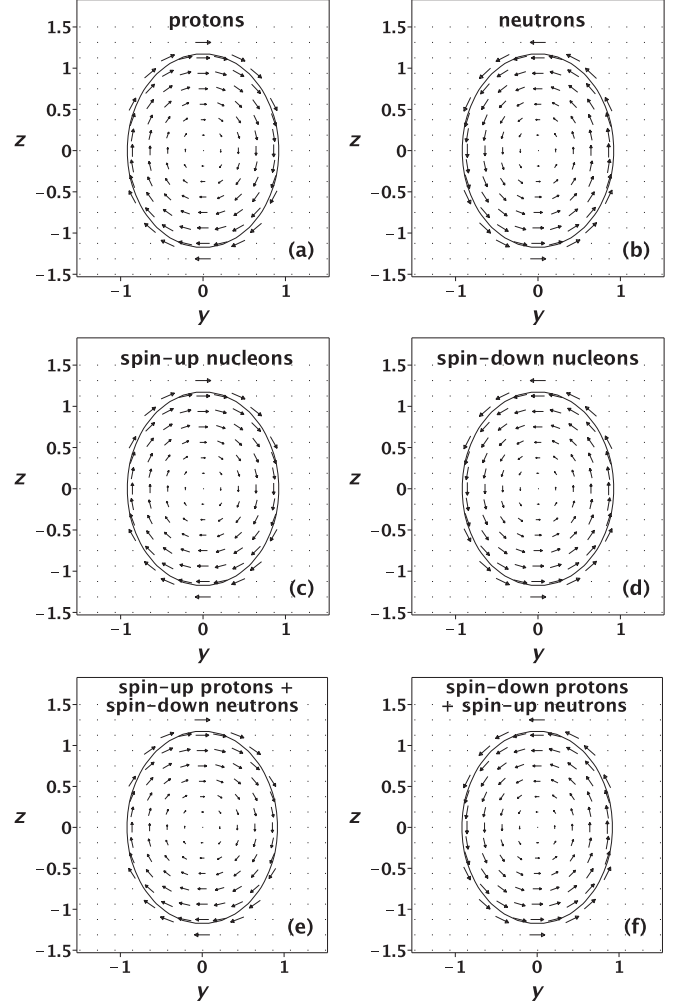
with rather big admixture (32%) of the conventional scissors [Figs. 10(a) and 10(b)].

(3) Excitation with $E = 3.59$ MeV represents predominantly (62%) the conventional scissors [Figs. 11(a) and 11(b)] with a rather strong admixture (31%) of the complicated spin scissors [Figs. 11(e) and 11(f)].

It is worth noting that the introduced in [10] indicator $\beta = -B/A$ works here too: if β is positive or negative the lines of current produce an ellipse or hyperbola.

A special comment is required for the situation in Figs. 9(a) and 9(b) where both currents turn in the same direction leading to the impression that the total angular momentum is not zero as it should be. We remark, however, that (i) this configuration has very little weight (1.75%) and (ii) total angular momentum zero is well conserved, the counter-rotation being performed by the motion of spins.

The situation with currents in actinides is exactly the same as in rare earths. The picture of currents in ^{232}Th is practically indistinguishable from that of ^{164}Dy.
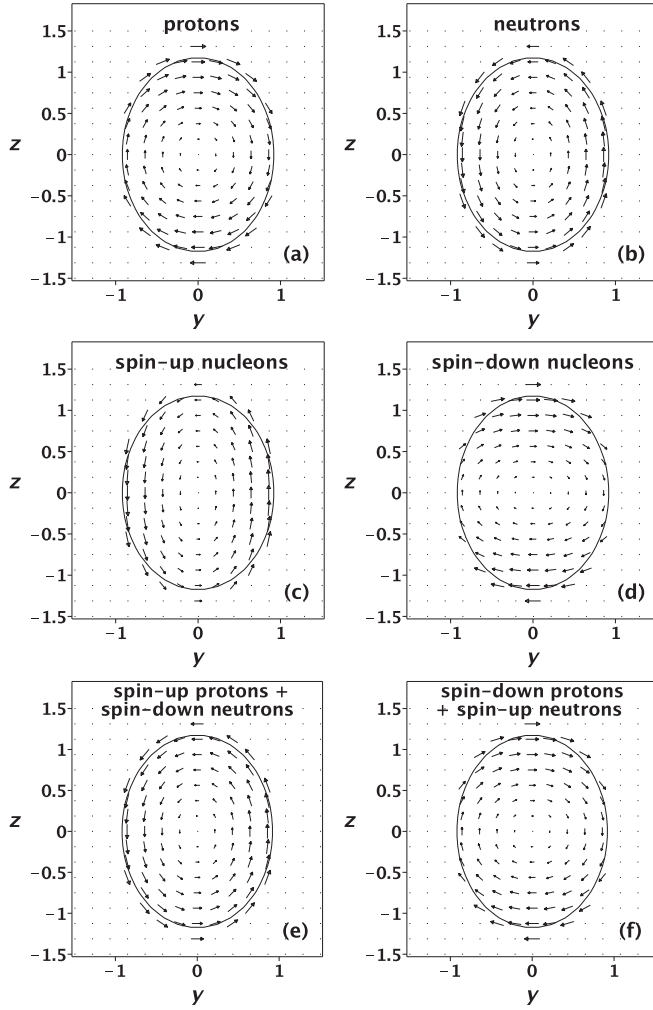
FIG. 11. The currents in ^{164}Dy for $E = 3.59$ MeV: δJ_p^+ (a), δJ_n^+ (b), $\delta J^{\uparrow\uparrow}$ (c), $\delta J^{\downarrow\downarrow}$ (d), $\delta J_p^{\uparrow\uparrow} + \delta J_n^{\downarrow\downarrow}$ (e), and $\delta J_p^{\downarrow\downarrow} + \delta J_n^{\uparrow\uparrow}$ (f). $\mathsf{y} = y/R$, $\mathsf{z} = z/R$.

TABLE VI. Strengths (amplitudes) of currents in ^{164}Dy. $\beta = -B/A$.

E (MeV)	(i)	B (10^{-2})	A (10^{-2})	%	β
	(a)	0.75	−0.47	1.75	1.60
	(b)	0.51	−0.18		2.79
2.20	(c)	−1.46	2.77	47.29	0.53
	(d)	2.72	−3.42		0.79
	(e)	2.87	−3.50	50.95	0.82
	(f)	−1.61	2.85		0.57
	(a)	1.99	−2.44	31.90	0.82
	(b)	−2.94	4.00		0.74
2.87	(c)	2.90	−3.32	53.71	0.87
	(d)	−3.85	4.89		0.79
	(e)	1.22	−1.24	14.39	0.99
	(f)	−2.17	2.80		0.78
	(a)	11.57	−12.14	61.55	0.95
	(b)	−8.17	15.05		0.54
3.59	(c)	−1.87	5.75	7.76	0.33
	(d)	5.27	−2.84		1.86
	(e)	−5.95	10.39	30.69	0.57
	(f)	9.35	−7.48		1.25

came to the conclusion that "the complexity of the observed spectrum originates from an interplay of the two mechanisms with one or the other dominating and a further fragmentation due to twists and other degrees of freedom." Herewith an important part of fragmentation is related to spin forces. At the same time, the signature for all actinides is negative. Such a result is in full agreement with the WFM theory. So the situation with respect to triaxiality is not yet completely clear. Though small triaxiality cannot be excluded from being responsible for some splitting of SR states in rare-earth nuclei, its inclusion in the present paper goes beyond its scope and we will postpone such a study for the future.

The interpretation of two excitations with energies 2.2 and 2.87 MeV as spin scissors is not obvious and requires some explanation. There are at least three questions to be answered.

IV. DISCUSSION

Palumbo analyzed the possible significance of triaxiality in explaining the fine structure of scissors resonance of the nuclei [38]. Indeed in [39] it is shown with a microscopic approach that only a very small triaxiality can induce the substantial splitting. Such a small triaxiality cannot be excluded to be present in ^{164}Dy. On the other hand the work in [39] is not free of deficiencies. Most importantly superfluidity is not included. This entails that for the moment of inertia the rigid body value is used while it is well known that its value is situated about halfway between the rigid and irrotational flow values (see [35]).

In discussing the splitting of SR, Palumbo introduced the so-called signature [38] that characterizes the energy partition in the treatment of [17]. Palumbo finds that in the rare-earth region the signature yields half positive and half negative values when the experimental values for $B(M1)$ values and energies given in [17] are taken. On the other hand WFM theory gives only negative values for the signature while the TRM approach in [38] leads to only positive values. Palumbo

A. Driving force

The first question is the following: what is the origin of forces which coerce the spin-up and spin-down particles to move out of phase? There is no analogous problem with the conventional scissors, because the Hamiltonian (5) includes the neutron-proton quadrupole-quadrupole interaction (6), which makes protons and neutrons move out of phase. But what generates a similar motion of spin-up and spin-down particles? It turns out that again the main working element is the nucleon-nucleon qq interaction. However, this time it works together with the spin-orbital part of the mean field.

Let us consider in detail the "life" of, for example, the system of spin-up protons and spin-down neutrons within the mean field. Due to the neutron-proton qq interaction, protons push neutrons and force them to move, generating in such a way for example the scissors modes [Fig. 2(b)]. Neutrons have spins, so due to the spin-orbital term their motion will depend on their spin projection. That means that the result of pushing
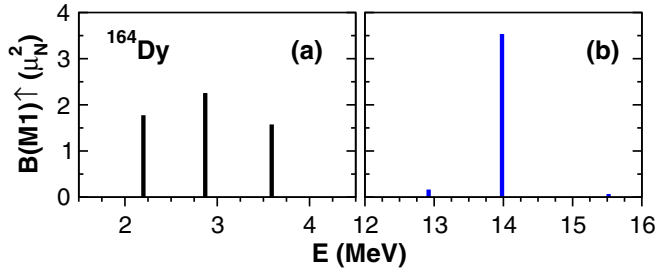
FIG. 12. Spectrum of $B(M1)$ strength distribution: (a) with nominal pairing strength and (b) with doubled pairing strength. Notice the very small satellites in panel (b).

will depend on the spin projections of the pushed neutrons. In addition, the pushing protons also have spins, therefore the result of pushing will depend on their spin projection too. Furthermore, due to proton-proton qq interaction spin-up protons will push spin-down protons and again the result of their interaction will be influenced by the spin-orbital potential. As we see, there is no necessity to introduce a special kind of interaction to activate the spin degrees of freedom and to generate in such a way the spin dependent excitations. It is done quite naturally by the usual qq interaction, the result of the activation being dependent on spin projections due to the spin-orbital potential, which can lead to the appearance of three different types of scissors motions.

B. Spin scissors versus Cooper pairs

The second question arises because it is sometimes mentioned that the low-lying spectrum of superfluid nuclei is entirely due to the motion of neutron and proton Cooper pairs. So, how can we have those spin scissors modes (b) and (c) of Fig. 2 when the spins of each species are locked into spin singlet Cooper pairs? The argument of spin-up and spin-down neutron and proton pairs locked in Cooper pairs would indeed be pertinent, if the two superfluids were ideal ones, expressed, e.g., by an irrotational moment of inertia. However, it is well known that the real moments of inertia are far from the irrotational limit, somewhere half in between the rigid body and irrotational value (see on this an illuminating recent work in [35]). For instance in that work velocity fields and moments of inertia are given by analytic formulas which divide these quantities into rotational and irrotational components. So, a good portion of the nucleons in deformed nuclei seems to be not paired but forming an unpaired four component Fermi gas. Of course, those effectively unpaired nucleons can make these spin scissors motion, since no force keeps, e.g., two neutrons locked into a spin-up/spin-down configuration. In order to underline this picture, we made the following very clarifying study. We artificially cranked up the pairing force. Then, of course, the nucleons' motion will become more and more irrotational and, thus, the standard scissors should become more and more preponderant. Well, that is exactly what is happening. Let us have a look at Fig. 12(a). There we show the spectrum of the three low-lying scissors states in ^{164}Dy for nominal pairing strength. As mentioned in Table I, they almost have equal $B(M1)$ values with the middle state slightly
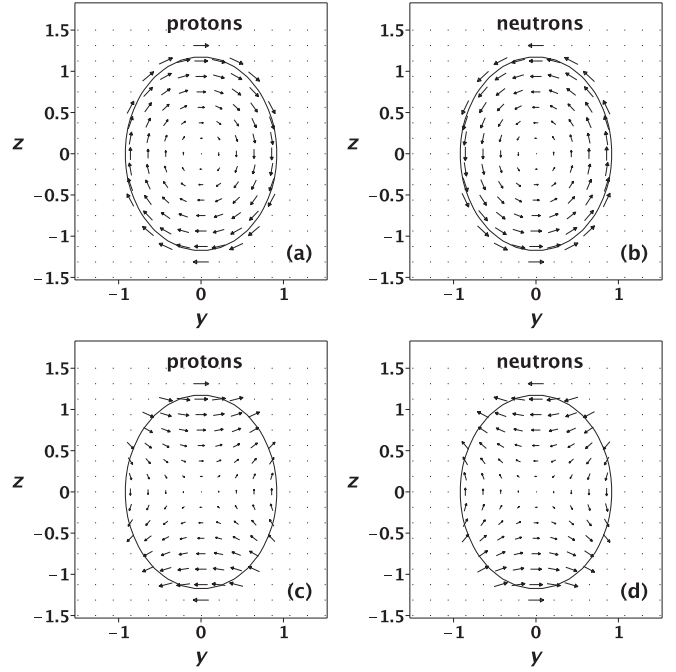

FIG. 13. (a, b) Flow patterns for the 2.87-MeV state with nominal pairing strength. (c, d) Flow patterns for the adiabatically connected state of panels (a) and (b) with doubled pairing strength.

sticking out having at the same time a large proportion of the standard scissors motion. Now on the right panel, the pairing strength is increased by a factor of 2. Not surprisingly the middle state has sucked up practically all $B(M1)$ strength with only a tiny strength remaining for the two satellites. Of course, the absolute value of the excitation energy has also strongly increased what is normal, since increased superfluidity makes the motion faster. We also show in Fig. 13 the flow patterns for the two situations. We see that in the case of nominal pairing strength the flows still reveal a good portion of rigid body motion whereas for the case of increased pairing strength the motion has become entirely irrotational, that is, bosonic with strongly bound pairs [40]. This study, therefore, highlights the fact that the picture of the scissors modes may be quite a bit more complicated than the usual idea of two counter-rotating proton and neutron distributions.

C. Spin scissors or spin flip?

A natural question which may arise is the relation of spin scissors with spin flip. As a matter of fact spin scissors and spin flip are just different names of the same physical phenomenon. From the microscopic [random-phase approximation (RPA)] point of view "spin flips" are transitions between spin-orbital partners. However, in present RPA calculations no analysis was made of what kind of orbital motion corresponds to these spin flips. Our study shows, that 1^+ excitations, described in RPA as spin flips, can be described by WFM as a counter-rotation of spin-up nucleons with respect to spin-down nucleons (i.e., spin scissors) because they belong to counteroscillations of their orbital angular momenta (see Figs. 9–11 for currents).

By the way, transitions between spin-orbital partners represent only the particular case among all possible transitions. Let us remember, for example, that from the microscopic point of view the conventional (orbital) scissors also are produced by transitions between some levels inside of one major shell (i.e., $\Delta N = 0$). The scissors-like nature of the considered excitation can be revealed by constructing the picture of currents or calculating the angular momenta of all four constituents (spin-up and spin-down protons and neutrons) of the excited nucleus.

The lines of currents are already produced in the WFM approach (see Figs. 9–11) Following our analysis, the spin and orbital low energy $M1$ excitations are strongly mixed. According to these results the energy area below 2.7 MeV in ^{164}Dy is mainly of the spin character. The analysis of currents allows one to conclude that the excitation with $E = 2.2$ MeV has an almost purely spin nature. Excitation with $E = 2.87$ MeV has a mixed structure: 68% of a spin nature and 32% of an orbital one. So, it is natural to expect that in the case of splitting of these two excitations the energy interval between them will be filled mainly by the excitations of the spin nature.

V. CONCLUSION

In this paper, we have solved the dynamical equations describing the nuclear collective scissors motion without the artificial decoupling of the isovector and isoscalar motions, an approximation we had applied in our previous work. As a result a new, third, type of nuclear scissors mode was found for which, however, there is a natural explanation. The three types of scissors modes can be approximately classified as isovector spin scalar (conventional), isovector spin vector, and isoscalar spin vector (see Fig. 2). Actually Fig. 2 is only a rough schematic view of the real situation. For this it is better to look at Figs. 9–11 which demonstrate the results of the calculations. The analysis of currents has shown that the three low-lying 1^+ magnetic excitations, predicted by the theory (see Table I), represent quite strong mixtures of all three scissors modes.

Since the motion in superfluid deformed nuclei is only halfway between rigid rotation and irrotational flow (see, e.g., [35]), this means that the pairing force is too weak to bind all nucleons into Cooper pairs. Therefore, one can consider (see [35]) that a good portion of the nucleons is still in a gaseous phase for which the excitation of spin scissors modes is very possible. On the other hand, we also have shown that in doubling the strength of the pairing force the flow becomes totally irrotational, implying that all nucleons are practically paired up. Not surprisingly, only the standard scissors mode of all protons swinging against all neutrons survives because of the very strongly bound Cooper pairs in this case.

A further very appreciable feature of the moment method should be mentioned: the eigenvalues have, mathematically speaking, the RPA property of $\pm$ degeneracy and show Goldstone (zero) modes in the case of spontaneously broken symmetries. That we obtain analytically a zero mode for broken rotational symmetry is a very strong sign of the performance of our 44 coupled equations (given in Appendix A), since otherwise this very sensitive zero mode would not appear at all. In conclusion, we may say that our second order moment equations yield an optimally coarse grained image of the full QRPA spectrum of the scissors modes. This is additionally born out in the remarkable agreement, seen in Fig. 6, of our $B(M1)$ transition probabilities with two QRPA results and with experimental values. A satisfactory agreement is also achieved for weakly deformed (transitional) nuclei of the same region by a very modest refit of the spin-orbit strength. We suppose that fourth order moments and more realistic interactions are required for the adequate description of transitional nuclei. The inclusion of (even small) triaxiality may also have some influence on the low-lying $M1$ spectra. These subjects shall be the objective of future work.

APPENDIX A: DYNAMICAL EQUATIONS

The set of dynamical equations for isovector variables reads

$$\dot{\mathcal{L}}_{21}^{+} = \frac{1}{m}\bar{\mathcal{P}}_{21}^{+} - [m\,\omega^2 + \kappa_0(4\alpha Q_{00} + (1+\alpha)Q_{20})]\bar{\mathcal{R}}_{21}^{+} - i\hbar\frac{\eta}{2}[\bar{\mathcal{L}}_{21}^{-} + 2\bar{\mathcal{L}}_{22}^{\uparrow\downarrow} + \sqrt{6}\bar{\mathcal{L}}_{20}^{\downarrow\uparrow}]$$

$$- \underbrace{\kappa_0(4\bar{Q}_{00} + (1+\alpha)\bar{Q}_{20})\mathcal{R}_{21}^{+}}_{\text{coupling term}},$$

$$\dot{\mathcal{L}}_{21}^{-} = \frac{1}{m}\bar{\mathcal{P}}_{21}^{-} - \left[m\,\omega^2 + \kappa_0 Q_{20} - \frac{\hbar^2}{15}(3\chi - \bar{\chi})\frac{I_1}{A_1 A_2}(Q_{00} + Q_{20}/4)\right]\bar{\mathcal{R}}_{21}^{-} - i\hbar\frac{\eta}{2}\bar{\mathcal{L}}_{21}^{+} + \frac{4}{\hbar}I_{rp}^{\kappa\Delta}(r')\bar{\bar{\mathcal{L}}}_{21}$$

$$- \underbrace{\left[\alpha\kappa_0\bar{Q}_{20} - \frac{\hbar^2}{15}(3\chi + \bar{\chi})\frac{I_1}{A_1 A_2}(\bar{Q}_{00} + \bar{Q}_{20}/4)\right]\mathcal{R}_{21}^{-}}_{} + \frac{4}{\hbar}\bar{I}_{rp}^{\kappa\Delta}(r')\tilde{\mathcal{L}}_{21},$$

$$\dot{\mathcal{L}}_{22}^{\uparrow\downarrow} = \frac{1}{m}\bar{\mathcal{P}}_{22}^{\uparrow\downarrow} - \left[m\,\omega^2 - 2\kappa_0 Q_{20} - 4\hbar^2(3\chi - \bar{\chi})\frac{I_1}{A_1 A_2}(Q_{20}+Q_{00})\right]\bar{\mathcal{R}}_{22}^{\uparrow\downarrow} - i\hbar\frac{\eta}{2}\bar{\mathcal{L}}_{21}^+$$

$$+ \underbrace{\left[2\alpha\kappa_0\bar{Q}_{20} + 4\hbar^2(3\chi + \bar{\chi})\frac{I_1}{A_1 A_2}(\bar{Q}_{20}+\bar{Q}_{00})\right]\mathcal{R}_{22}^{\uparrow\downarrow}},$$

$$\dot{\mathcal{L}}_{20}^{\downarrow\uparrow} = \frac{1}{m}\bar{\mathcal{P}}_{20}^{\downarrow\uparrow} - [m\,\omega^2 + 2\kappa_0 Q_{20}]\bar{\mathcal{R}}_{20}^{\downarrow\uparrow} + 2\sqrt{2}\kappa_0 Q_{20}\,\bar{\mathcal{R}}_{00}^{\downarrow\uparrow} - i\hbar\frac{\eta}{2}\sqrt{\frac{3}{2}}\bar{\mathcal{L}}_{21}^+$$

$$+ \frac{\hbar^2}{15}(3\chi - \bar{\chi})\frac{I_1}{A_1 A_2}[Q_{00}\bar{\mathcal{R}}_{20}^{\downarrow\uparrow} + Q_{20}\bar{\mathcal{R}}_{00}^{\downarrow\uparrow}/\sqrt{2}]$$

$$\underbrace{-2\alpha\kappa_0\bar{Q}_{20}[\mathcal{R}_{20}^{\downarrow\uparrow} + \sqrt{2}\mathcal{R}_{00}^{\downarrow\uparrow}] + \frac{\hbar^2}{15}(3\chi + \bar{\chi})\frac{I_1}{A_1 A_2}[\bar{Q}_{00}\mathcal{R}_{20}^{\downarrow\uparrow} + \bar{Q}_{20}\mathcal{R}_{00}^{\downarrow\uparrow}/\sqrt{2}]},$$

$$\dot{\mathcal{L}}_{11}^+ = -3(1-\alpha)\kappa_0 Q_{20}\,\bar{\mathcal{R}}_{21}^+ - i\hbar\frac{\eta}{2}[\bar{\mathcal{L}}_{11}^- + \sqrt{2}\bar{\mathcal{L}}_{10}^{\downarrow\uparrow}] + \underbrace{3(1-\alpha)\kappa_0\bar{Q}_{20}\,\mathcal{R}_{21}^+},$$

$$\dot{\mathcal{L}}_{11}^- = -\left[3\kappa_0 Q_{20} + \frac{\hbar^2}{20}(3\chi - \bar{\chi})\frac{I_1}{A_1 A_2}Q_{20}\right]\bar{\mathcal{R}}_{21}^- + \frac{4}{\hbar}I_{rp}^{\kappa\Delta}(r')\bar{\bar{\mathcal{L}}}_{11} - \hbar\frac{\eta}{2}[i\bar{\mathcal{L}}_{11}^+ + \hbar\bar{\mathcal{F}}^{\downarrow\uparrow}]$$

$$-\underbrace{\left[3\alpha\kappa_0\bar{Q}_{20} + \frac{\hbar^2}{20}(3\chi + \bar{\chi})\frac{I_1}{A_1 A_2}\bar{Q}_{20}\right]\mathcal{R}_{21}^- + \frac{4}{\hbar}\bar{I}_{rp}^{\kappa\Delta}(r')\tilde{\mathcal{L}}_{11}},$$

$$\dot{\mathcal{L}}_{10}^{\downarrow\uparrow} = -\hbar\frac{\eta}{2\sqrt{2}}[i\bar{\mathcal{L}}_{11}^+ + \hbar\bar{\mathcal{F}}^{\downarrow\uparrow}],$$

$$\dot{\mathcal{F}}^{\downarrow\uparrow} = -\eta[\bar{\mathcal{L}}_{11}^- + \sqrt{2}\bar{\mathcal{L}}_{10}^{\downarrow\uparrow}],$$

$$\dot{\mathcal{R}}_{21}^+ = \frac{2}{m}\bar{\mathcal{L}}_{21}^+ - i\hbar\frac{\eta}{2}[\bar{\mathcal{R}}_{21}^- + 2\bar{\mathcal{R}}_{22}^{\uparrow\downarrow} + \sqrt{6}\bar{\mathcal{R}}_{20}^{\downarrow\uparrow}],$$

$$\dot{\mathcal{R}}_{21}^- = \frac{2}{m}\bar{\mathcal{L}}_{21}^- - i\hbar\frac{\eta}{2}\bar{\mathcal{R}}_{21}^+,$$

$$\dot{\mathcal{R}}_{22}^{\uparrow\downarrow} = \frac{2}{m}\bar{\mathcal{L}}_{22}^{\uparrow\downarrow} - i\hbar\frac{\eta}{2}\bar{\mathcal{R}}_{21}^+,$$

$$\dot{\mathcal{R}}_{20}^{\downarrow\uparrow} = \frac{2}{m}\bar{\mathcal{L}}_{20}^{\downarrow\uparrow} - i\hbar\frac{\eta}{2}\sqrt{\frac{3}{2}}\bar{\mathcal{R}}_{21}^+,$$

$$\dot{\mathcal{P}}_{21}^+ = -2[m\,\omega^2 + \kappa_0 Q_{20}]\bar{\mathcal{L}}_{21}^+ + 6\kappa_0 Q_{20}\bar{\mathcal{L}}_{11}^+ - i\hbar\frac{\eta}{2}[\bar{\mathcal{P}}_{21}^- + 2\bar{\mathcal{P}}_{22}^{\uparrow\downarrow} + \sqrt{6}\bar{\mathcal{P}}_{20}^{\downarrow\uparrow}]$$

$$+ \frac{3}{8}\hbar^2\chi\frac{I_2}{A_1 A_2}[(Q_{20}+4Q_{00})\bar{\mathcal{L}}_{21}^+ + 3Q_{20}\bar{\mathcal{L}}_{11}^+] + \frac{4}{\hbar}I_{pp}^{\kappa\Delta}(r')\bar{\bar{\mathcal{P}}}_{21}$$

$$+ \underbrace{2\alpha\kappa_0\bar{Q}_{20}(3\mathcal{L}_{11}^+ - \mathcal{L}_{21}^+) + \frac{3}{8}\hbar^2\chi\frac{I_2}{A_1 A_2}[(\bar{Q}_{20}+4\bar{Q}_{00})\mathcal{L}_{21}^+ + 3\bar{Q}_{20}\mathcal{L}_{11}^+] + \frac{4}{\hbar}\bar{I}_{pp}^{\kappa\Delta}(r')\tilde{\mathcal{P}}_{21}},$$

$$\dot{\mathcal{P}}_{21}^- = -2[m\,\omega^2 + \kappa_0 Q_{20}]\bar{\mathcal{L}}_{21}^- + 6\kappa_0 Q_{20}\bar{\mathcal{L}}_{11}^- - 6\sqrt{2}\alpha\kappa_0 L_{10}^-(\mathrm{eq})\bar{\mathcal{R}}_{21}^+ - i\hbar\frac{\eta}{2}\bar{\mathcal{P}}_{21}^+$$

$$+ \frac{3}{8}\hbar^2\chi\frac{I_2}{A_1 A_2}[(Q_{20}+4Q_{00})\bar{\mathcal{L}}_{21}^- + 3Q_{20}\bar{\mathcal{L}}_{11}^-]$$

$$+ \underbrace{2\alpha\kappa_0\bar{Q}_{20}(3\mathcal{L}_{11}^- - \mathcal{L}_{21}^-) + \frac{3}{8}\hbar^2\chi\frac{I_2}{A_1 A_2}[(\bar{Q}_{20}+4\bar{Q}_{00})\mathcal{L}_{21}^- + 3\bar{Q}_{20}\mathcal{L}_{11}^-] - 6\sqrt{2}\kappa_0\bar{L}_{10}^-(\mathrm{eq})\mathcal{R}_{21}^+},$$

$$\dot{\mathcal{P}}_{22}^{\uparrow\downarrow} = -2[m\,\omega^2 - 2\kappa_0 Q_{20}]\bar{\mathcal{L}}_{22}^{\uparrow\downarrow} - i\hbar\frac{\eta}{2}\bar{\mathcal{P}}_{21}^+ + \frac{3}{2}\hbar^2\chi\frac{I_2}{A_1 A_2}(Q_{20}+Q_{00})\bar{\mathcal{L}}_{22}^{\uparrow\downarrow}$$

$$+ \underbrace{4\alpha\kappa_0\bar{Q}_{20}\mathcal{L}_{22}^{\uparrow\downarrow} + \frac{3}{2}\hbar^2\chi\frac{I_2}{A_1 A_2}(\bar{Q}_{20}+\bar{Q}_{00})\mathcal{L}_{22}^{\uparrow\downarrow}},$$

$$
\dot{\mathcal{P}}_{20}^{\downarrow\uparrow} = -2[m\,\omega^2 + 2\kappa_0 Q_{20}]\bar{\mathcal{L}}_{20}^{\downarrow\uparrow} + 4\sqrt{2}\kappa_0 Q_{20}\bar{\mathcal{L}}_{00}^{\downarrow\uparrow} - i\hbar\frac{\eta}{2}\sqrt{\frac{3}{2}}\bar{\mathcal{P}}_{21}^+ + \frac{3}{2}\hbar^2\chi\frac{I_2}{A_1 A_2}[Q_{00}\bar{\mathcal{L}}_{20}^{\downarrow\uparrow} + Q_{20}\bar{\mathcal{L}}_{00}^{\downarrow\uparrow}/\sqrt{2}]
$$

$$
+ 4\alpha\kappa_0\bar{Q}_{20}(\sqrt{2}\mathcal{L}_{00}^{\downarrow\uparrow} - \mathcal{L}_{20}^{\downarrow\uparrow}) + \underbrace{\frac{3}{2}\hbar^2\chi\frac{I_2}{A_1 A_2}[\bar{Q}_{00}\mathcal{L}_{20}^{\downarrow\uparrow} + \bar{Q}_{20}\mathcal{L}_{00}^{\downarrow\uparrow}/\sqrt{2}]},
$$

$$
\dot{\mathcal{L}}_{00}^{\downarrow\uparrow} = \frac{1}{m}\bar{\mathcal{P}}_{00}^{\downarrow\uparrow} - m\,\omega^2 \bar{\mathcal{R}}_{00}^{\downarrow\uparrow} + 2\sqrt{2}\kappa_0 Q_{20}\bar{\mathcal{R}}_{20}^{\downarrow\uparrow} + \frac{\hbar^2}{4 A_1 A_2}\left[\left(\chi - \frac{\bar{\chi}}{3}\right)I_1 - \frac{9}{4}\chi I_2\right][(2Q_{00} + Q_{20})\bar{\mathcal{R}}_{00}^{\downarrow\uparrow} + \sqrt{2}Q_{20}\bar{\mathcal{R}}_{20}^{\downarrow\uparrow}]
$$

$$
+ 2\sqrt{2}\alpha\kappa_0\bar{Q}_{20}\mathcal{R}_{20}^{\downarrow\uparrow} + \underbrace{\frac{\hbar^2}{4 A_1 A_2}\left[\left(\chi + \frac{\bar{\chi}}{3}\right)I_1 - \frac{9}{4}\chi I_2\right][(2\bar{Q}_{00} + \bar{Q}_{20})\mathcal{R}_{00}^{\downarrow\uparrow} + \sqrt{2}\bar{Q}_{20}\mathcal{R}_{20}^{\downarrow\uparrow}]},
$$

$$
\dot{\mathcal{R}}_{00}^{\downarrow\uparrow} = \frac{2}{m}\bar{\mathcal{L}}_{00}^{\downarrow\uparrow},
$$

$$
\dot{\mathcal{P}}_{00}^{\downarrow\uparrow} = -2m\,\omega^2\bar{\mathcal{L}}_{00}^{\downarrow\uparrow} + 4\sqrt{2}\kappa_0 Q_{20}\bar{\mathcal{L}}_{20}^{\downarrow\uparrow} + \frac{3}{4}\hbar^2\chi\frac{I_2}{A_1 A_2}[(2Q_{00} + Q_{20})\bar{\mathcal{L}}_{00}^{\downarrow\uparrow} + \sqrt{2}Q_{20}\bar{\mathcal{L}}_{20}^{\downarrow\uparrow}]
$$

$$
+ 4\sqrt{2}\alpha\kappa_0\bar{Q}_{20}\mathcal{L}_{20}^{\downarrow\uparrow} + \underbrace{\frac{3}{4}\hbar^2\chi\frac{I_2}{A_1 A_2}[(2\bar{Q}_{00} + \bar{Q}_{20})\mathcal{L}_{00}^{\downarrow\uparrow} + \sqrt{2}\bar{Q}_{20}\mathcal{L}_{20}^{\downarrow\uparrow}]},
$$

$$
\dot{\bar{\mathcal{P}}}_{21} = -\frac{1}{2\hbar}\Delta(r')\bar{\mathcal{P}}_{21}^+ + 6\hbar\alpha\kappa_0 K_0\bar{\mathcal{R}}_{21}^+ \underbrace{-\frac{1}{2\hbar}\bar{\Delta}(r')\mathcal{P}_{21}^+ + 6\hbar\kappa_0\bar{K}_0\mathcal{R}_{21}^+},
$$

$$
\dot{\bar{\mathcal{L}}}_{21} = -\frac{1}{2\hbar}\Delta(r')\bar{\mathcal{L}}_{21}^- \underbrace{-\frac{1}{2\hbar}\bar{\Delta}(r')\mathcal{L}_{21}^-},
$$

$$
\dot{\bar{\mathcal{L}}}_{11} = -\frac{1}{2\hbar}\Delta(r')\bar{\mathcal{L}}_{11}^- \underbrace{-\frac{1}{2\hbar}\bar{\Delta}(r')\mathcal{L}_{11}^-}. \tag{A1}
$$

The set of dynamical equations for isoscalar variables reads

$$
\dot{\mathcal{L}}_{21}^+ = \frac{1}{m}\mathcal{P}_{21}^+ - [m\,\omega^2 + 2\kappa_0(2Q_{00} + Q_{20})]\mathcal{R}_{21}^+ - i\hbar\frac{\eta}{2}[\mathcal{L}_{21}^- + 2\mathcal{L}_{22}^{\uparrow\downarrow} + \sqrt{6}\mathcal{L}_{20}^{\downarrow\uparrow}] - \underbrace{\alpha\kappa_0(2\bar{Q}_{00} + \bar{Q}_{20})\bar{\mathcal{R}}_{21}^+}_{\text{coupling term}},
$$

$$
\dot{\mathcal{L}}_{21}^- = \frac{1}{m}\mathcal{P}_{21}^- - \left[m\,\omega^2 + \kappa_0 Q_{20} - \frac{\hbar^2}{15}(3\chi + \bar{\chi})\frac{I_1}{A_1 A_2}(Q_{00} + Q_{20}/4)\right]\mathcal{R}_{21}^- - i\hbar\frac{\eta}{2}\mathcal{L}_{21}^+ + \frac{4}{\hbar}I_{rp}^{\kappa\Delta}(r')\tilde{\mathcal{L}}_{21}
$$

$$
- \underbrace{\left[\alpha\kappa_0\bar{Q}_{20} - \frac{\hbar^2}{15}(3\chi - \bar{\chi})\frac{I_1}{A_1 A_2}(\bar{Q}_{00} + \bar{Q}_{20}/4)\right]\bar{\mathcal{R}}_{21}^- + \frac{4}{\hbar}\bar{I}_{rp}^{\kappa\Delta}(r')\bar{\tilde{\mathcal{L}}}_{21}},
$$

$$
\dot{\mathcal{L}}_{22}^{\uparrow\downarrow} = \frac{1}{m}\mathcal{P}_{22}^{\uparrow\downarrow} - \left[m\,\omega^2 - 2\kappa_0 Q_{20} - 4\hbar^2(3\chi + \bar{\chi})\frac{I_1}{A_1 A_2}(Q_{20} + Q_{00})\right]\mathcal{R}_{22}^{\uparrow\downarrow} - i\hbar\frac{\eta}{2}\mathcal{L}_{21}^+
$$

$$
+ \underbrace{\left[2\alpha\kappa_0\bar{Q}_{20} + 4\hbar^2(3\chi - \bar{\chi})\frac{I_1}{A_1 A_2}(\bar{Q}_{20} + \bar{Q}_{00})\right]\bar{\mathcal{R}}_{22}^{\uparrow\downarrow}},
$$

$$
\dot{\mathcal{L}}_{20}^{\downarrow\uparrow} = \frac{1}{m}\mathcal{P}_{20}^{\downarrow\uparrow} - [m\,\omega^2 + 2\kappa_0 Q_{20}]\mathcal{R}_{20}^{\downarrow\uparrow} + 2\sqrt{2}\kappa_0 Q_{20}\,\mathcal{R}_{00}^{\downarrow\uparrow} - i\hbar\frac{\eta}{2}\sqrt{\frac{3}{2}}\mathcal{L}_{21}^+
$$

$$
+ \frac{\hbar^2}{15}(3\chi + \bar{\chi})\frac{I_1}{A_1 A_2}[Q_{00}\mathcal{R}_{20}^{\downarrow\uparrow} + Q_{20}\mathcal{R}_{00}^{\downarrow\uparrow}/\sqrt{2}]
$$

$$
\underbrace{-2\alpha\kappa_0\bar{Q}_{20}[\bar{\mathcal{R}}_{20}^{\downarrow\uparrow} + \sqrt{2}\bar{\mathcal{R}}_{00}^{\downarrow\uparrow}] + \frac{\hbar^2}{15}(3\chi - \bar{\chi})\frac{I_1}{A_1 A_2}[\bar{Q}_{00}\bar{\mathcal{R}}_{20}^{\downarrow\uparrow} + \bar{Q}_{20}\bar{\mathcal{R}}_{00}^{\downarrow\uparrow}/\sqrt{2}]},
$$

$$
\dot{\mathcal{L}}_{11}^+ = -i\hbar\frac{\eta}{2}[\mathcal{L}_{11}^- + \sqrt{2}\mathcal{L}_{10}^{\downarrow\uparrow}],
$$

$$\dot{\mathcal{L}}_{11}^- = -\left[3\kappa_0 Q_{20} + \frac{\hbar^2}{20}(3\chi + \bar{\chi})\frac{I_1}{A_1 A_2}Q_{20}\right]\mathcal{R}_{21}^- + \frac{4}{\hbar}I_{rp}^{\kappa\Delta}(r')\tilde{\mathcal{L}}_{11} - \hbar\frac{\eta}{2}[i\mathcal{L}_{11}^+ + \hbar\mathcal{F}^{\downarrow\uparrow}]$$

$$- \underbrace{\left[3\alpha\kappa_0\bar{Q}_{20} + \frac{\hbar^2}{20}(3\chi - \bar{\chi})\frac{I_1}{A_1 A_2}\bar{Q}_{20}\right]\bar{\mathcal{R}}_{21}^- + \frac{4}{\hbar}\bar{I}_{rp}^{\kappa\Delta}(r')\bar{\tilde{\mathcal{L}}}_{11}},$$

$$\dot{\mathcal{L}}_{10}^{\downarrow\uparrow} = -\hbar\frac{\eta}{2\sqrt{2}}[i\mathcal{L}_{11}^+ + \hbar\mathcal{F}^{\downarrow\uparrow}],$$

$$\dot{\mathcal{F}}^{\downarrow\uparrow} = -\eta[\mathcal{L}_{11}^- + \sqrt{2}\mathcal{L}_{10}^{\downarrow\uparrow}],$$

$$\dot{\mathcal{R}}_{21}^+ = \frac{2}{m}\mathcal{L}_{21}^+ - i\hbar\frac{\eta}{2}[\mathcal{R}_{21}^- + 2\mathcal{R}_{22}^{\uparrow\downarrow} + \sqrt{6}\mathcal{R}_{20}^{\downarrow\uparrow}],$$

$$\dot{\mathcal{R}}_{21}^- = \frac{2}{m}\mathcal{L}_{21}^- - i\hbar\frac{\eta}{2}\mathcal{R}_{21}^+,$$

$$\dot{\mathcal{R}}_{22}^{\uparrow\downarrow} = \frac{2}{m}\mathcal{L}_{22}^{\uparrow\downarrow} - i\hbar\frac{\eta}{2}\mathcal{R}_{21}^+,$$

$$\dot{\mathcal{R}}_{20}^{\downarrow\uparrow} = \frac{2}{m}\mathcal{L}_{20}^{\downarrow\uparrow} - i\hbar\frac{\eta}{2}\sqrt{\frac{3}{2}}\mathcal{R}_{21}^+,$$

$$\dot{\mathcal{P}}_{21}^+ = -2[m\omega^2 + \kappa_0 Q_{20}]\mathcal{L}_{21}^+ + 6\kappa_0 Q_{20}\mathcal{L}_{11}^+ - i\hbar\frac{\eta}{2}[\mathcal{P}_{21}^- + 2\mathcal{P}_{22}^{\uparrow\downarrow} + \sqrt{6}\mathcal{P}_{20}^{\downarrow\uparrow}]$$

$$+ \frac{3}{8}\hbar^2\chi\frac{I_2}{A_1 A_2}[(Q_{20} + 4Q_{00})\mathcal{L}_{21}^+ + 3Q_{20}\mathcal{L}_{11}^+] + \frac{4}{\hbar}I_{pp}^{\kappa\Delta}(r')\tilde{\mathcal{P}}_{21}$$

$$+ 2\alpha\kappa_0\bar{Q}_{20}(3\bar{\mathcal{L}}_{11}^+ - \bar{\mathcal{L}}_{21}^+) + \frac{3}{8}\hbar^2\chi\frac{I_2}{A_1 A_2}[(\bar{Q}_{20} + 4\bar{Q}_{00})\bar{\mathcal{L}}_{21}^+ + 3\bar{Q}_{20}\bar{\mathcal{L}}_{11}^+] + \frac{4}{\hbar}\bar{I}_{pp}^{\kappa\Delta}(r')\bar{\tilde{\mathcal{P}}}_{21},$$

$$\dot{\mathcal{P}}_{21}^- = -2[m\omega^2 + \kappa_0 Q_{20}]\mathcal{L}_{21}^- + 6\kappa_0 Q_{20}\mathcal{L}_{11}^- - 6\sqrt{2}\kappa_0 L_{10}(\text{eq})\mathcal{R}_{21}^+ - i\hbar\frac{\eta}{2}\mathcal{P}_{21}^+$$

$$+ \frac{3}{8}\hbar^2\chi\frac{I_2}{A_1 A_2}[(Q_{20} + 4Q_{00})\mathcal{L}_{21}^- + 3Q_{20}\mathcal{L}_{11}^-]$$

$$+ 2\alpha\kappa_0\bar{Q}_{20}(3\bar{\mathcal{L}}_{11}^- - \bar{\mathcal{L}}_{21}^-) + \frac{3}{8}\hbar^2\chi\frac{I_2}{A_1 A_2}[(\bar{Q}_{20} + 4\bar{Q}_{00})\bar{\mathcal{L}}_{21}^- + 3\bar{Q}_{20}\bar{\mathcal{L}}_{11}^-] - 6\sqrt{2}\alpha\kappa_0\bar{L}_{10}^-(\text{eq})\bar{\mathcal{R}}_{21}^+,$$

$$\dot{\mathcal{P}}_{22}^{\uparrow\downarrow} = -2[m\omega^2 - 2\kappa_0 Q_{20}]\mathcal{L}_{22}^{\uparrow\downarrow} - i\hbar\frac{\eta}{2}\mathcal{P}_{21}^+ + \frac{3}{2}\hbar^2\chi\frac{I_2}{A_1 A_2}(Q_{20} + Q_{00})\mathcal{L}_{22}^{\uparrow\downarrow}$$

$$+ 4\alpha\kappa_0\bar{Q}_{20}\bar{\mathcal{L}}_{22}^{\uparrow\downarrow} + \frac{3}{2}\hbar^2\chi\frac{I_2}{A_1 A_2}(\bar{Q}_{20} + \bar{Q}_{00})\bar{\mathcal{L}}_{22}^{\uparrow\downarrow},$$

$$\dot{\mathcal{P}}_{20}^{\downarrow\uparrow} = -2[m\omega^2 + 2\kappa_0 Q_{20}]\mathcal{L}_{20}^{\downarrow\uparrow} + 4\sqrt{2}\kappa_0 Q_{20}\mathcal{L}_{00}^{\downarrow\uparrow} - i\hbar\frac{\eta}{2}\sqrt{\frac{3}{2}}\mathcal{P}_{21}^+ + \frac{3}{2}\hbar^2\chi\frac{I_2}{A_1 A_2}[Q_{00}\mathcal{L}_{20}^{\downarrow\uparrow} + Q_{20}\mathcal{L}_{00}^{\downarrow\uparrow}/\sqrt{2}]$$

$$+ 4\alpha\kappa_0\bar{Q}_{20}(\sqrt{2}\bar{\mathcal{L}}_{00}^{\downarrow\uparrow} - \bar{\mathcal{L}}_{20}^{\downarrow\uparrow}) + \frac{3}{2}\hbar^2\chi\frac{I_2}{A_1 A_2}[\bar{Q}_{00}\bar{\mathcal{L}}_{20}^{\downarrow\uparrow} + \bar{Q}_{20}\bar{\mathcal{L}}_{00}^{\downarrow\uparrow}/\sqrt{2}],$$

$$\dot{\mathcal{L}}_{00}^{\downarrow\uparrow} = \frac{1}{m}\mathcal{P}_{00}^{\downarrow\uparrow} - m\omega^2\mathcal{R}_{00}^{\downarrow\uparrow} + 2\sqrt{2}\kappa_0 Q_{20}\mathcal{R}_{20}^{\downarrow\uparrow} + \frac{\hbar^2}{4A_1 A_2}\left[\left(\chi + \frac{\bar{\chi}}{3}\right)I_1 - \frac{9}{4}\chi I_2\right][(2Q_{00} + Q_{20})\mathcal{R}_{00}^{\downarrow\uparrow} + \sqrt{2}Q_{20}\mathcal{R}_{20}^{\downarrow\uparrow}]$$

$$+ 2\sqrt{2}\alpha\kappa_0\bar{Q}_{20}\bar{\mathcal{R}}_{20}^{\downarrow\uparrow} + \frac{\hbar^2}{4A_1 A_2}\left[\left(\chi - \frac{\bar{\chi}}{3}\right)I_1 - \frac{9}{4}\chi I_2\right][(2\bar{Q}_{00} + \bar{Q}_{20})\bar{\mathcal{R}}_{00}^{\downarrow\uparrow} + \sqrt{2}\bar{Q}_{20}\bar{\mathcal{R}}_{20}^{\downarrow\uparrow}],$$

$$\dot{\mathcal{R}}_{00}^{\downarrow\uparrow} = \frac{2}{m}\mathcal{L}_{00}^{\downarrow\uparrow},$$

$$\dot{\mathcal{P}}_{00}^{\downarrow\uparrow} = -2m\omega^2\mathcal{L}_{00}^{\downarrow\uparrow} + 4\sqrt{2}\kappa_0 Q_{20}\mathcal{L}_{20}^{\downarrow\uparrow} + \frac{3}{4}\hbar^2\chi\frac{I_2}{A_1 A_2}[(2Q_{00} + Q_{20})\bar{\mathcal{L}}_{00}^{\downarrow\uparrow} + \sqrt{2}Q_{20}\bar{\mathcal{L}}_{20}^{\downarrow\uparrow}]$$

$$+ 4\sqrt{2}\alpha\kappa_0\bar{Q}_{20}\bar{\mathcal{L}}_{20}^{\downarrow\uparrow} + \frac{3}{4}\hbar^2\chi\frac{I_2}{A_1 A_2}[(2\bar{Q}_{00} + \bar{Q}_{20})\bar{\mathcal{L}}_{00}^{\downarrow\uparrow} + \sqrt{2}\bar{Q}_{20}\bar{\mathcal{L}}_{20}^{\downarrow\uparrow}],$$

$$\dot{\mathcal{P}}_{21} = -\frac{1}{2\hbar}\Delta(r')\mathcal{P}_{21}^+ + 6\hbar\kappa_0 K_0\mathcal{R}_{21}^+ \underbrace{-\frac{1}{2\hbar}\bar{\Delta}(r')\bar{\mathcal{P}}_{21}^+ + 6\hbar\alpha\kappa_0\bar{K}_0\bar{\mathcal{R}}_{21}^+},$$

$$\dot{\mathcal{L}}_{21} = -\frac{1}{2\hbar}\Delta(r')\mathcal{L}_{21}^- \underbrace{-\frac{1}{2\hbar}\bar{\Delta}(r')\bar{\mathcal{L}}_{21}^-},$$

$$\dot{\mathcal{L}}_{11} = -\frac{1}{2\hbar}\Delta(r')\mathcal{L}_{11}^- \underbrace{-\frac{1}{2\hbar}\bar{\Delta}(r')\bar{\mathcal{L}}_{11}^-}, \tag{A2}$$

where the terms coupling isovector and isoscalar sets of equations are underlined by the braces and

$$A_1 = \sqrt{2}\,R_{20}^{\text{eq}} - R_{00}^{\text{eq}} = \frac{Q_{00}}{\sqrt{3}}\left(1 + \frac{4}{3}\delta\right), \quad A_2 = R_{20}^{\text{eq}}/\sqrt{2} + R_{00}^{\text{eq}} = -\frac{Q_{00}}{\sqrt{3}}\left(1 - \frac{2}{3}\delta\right), \tag{A3}$$

$Q_{00} = \frac{3}{5}AR^2/[(1 + \frac{4}{3}\delta)^{1/3}(1 - \frac{2}{3}\delta)^{2/3}]$, δ is the deformation parameter, $Q_{20} = \frac{4}{3}\delta Q_{00}$, $\bar{Q}_{00} = Q_{00}^n - Q_{00}^p$, $\bar{Q}_{20} = Q_{20}^n - Q_{20}^p$, $\bar{\Delta} = \Delta^n - \Delta^p$, $\Delta = \Delta^n + \Delta^p$, $R = r_0 A^{1/3}$, $r_0 = 1.2$ fm,

$$I_1 = \frac{\pi}{4}\int_0^\infty dr\, r^4\left(\frac{\partial n(r)}{\partial r}\right)^2, \quad I_2 = \frac{\pi}{4}\int_0^\infty dr\, r^2 n(r)^2, \quad K_0^\tau = \int d(\mathbf{r}, \mathbf{p})\kappa_0^\tau(\mathbf{r}, \mathbf{p}),$$

$\bar{K}_0 = K_0^n - K_0^p$, $K_0 = K_0^n + K_0^p$, $n(r) = n_0(1 + e^{\frac{r-R}{a}})^{-1}$ is nuclear density, and $a = 0.53$ fm. Further, $I_{pp}^{\kappa\Delta}(\mathbf{r}, p) = |V_0|\frac{r_p^3}{\sqrt{\pi}\hbar^3}e^{-\alpha p^2}\int\kappa^r(\mathbf{r}, p')[\phi_0(x) - 4\alpha^2 p'^4\phi_2(x)]e^{-\alpha p'^2}p'^2 dp'$, and $I_{rp}^{\kappa\Delta}(\mathbf{r}, p) = |V_0|\frac{r_p^3}{\sqrt{\pi}\hbar^3}e^{-\alpha p^2}\int\kappa^r(\mathbf{r}, p')[\phi_0(x) - 2\alpha p'^2\phi_1(x)]e^{-\alpha p'^2}p'^2 dp'$, where $x = 2\alpha pp'$, $\phi_0(x) = \frac{1}{x}\sinh(x)$, $\phi_1(x) = \frac{1}{x^2}[\cosh(x) - \frac{1}{x}\sinh(x)]$, and $\phi_2(x) = \frac{1}{x^3}[(1 + \frac{3}{x^2})\sinh(x) - \frac{3}{x}\cosh(x)]$.

Anomalous density and semiclassical gap equations [15] read

$$\kappa(\mathbf{r}, \mathbf{p}) = \frac{1}{2}\frac{\Delta(\mathbf{r}, \mathbf{p})}{\sqrt{h^2(\mathbf{r}, \mathbf{p}) + \Delta^2(\mathbf{r}, \mathbf{p})}}, \tag{A4}$$

$$\Delta(\mathbf{r}, \mathbf{p}) = -\frac{1}{2}\int\frac{d^3 p'}{(2\pi\hbar)^3}v(|\mathbf{p} - \mathbf{p}'|)\frac{\Delta(\mathbf{r}, \mathbf{p}')}{\sqrt{h^2(\mathbf{r}, \mathbf{p}') + \Delta^2(\mathbf{r}, \mathbf{p}')}}, \tag{A5}$$

where $v(|\mathbf{p} - \mathbf{p}'|) = \beta e^{-\alpha|\mathbf{p}-\mathbf{p}'|^2}$ with $\beta = -|V_0|(r_p\sqrt{\pi})^3$ and $\alpha = r_p^2/4\hbar^2$.

Parameters of pair correlations for WFM calculations read $V_0^p = 27$ MeV, $V_0^n = 23$ MeV, $r_p^p = 1.50$ fm, and $r_p^n = 1.85$ fm for nuclei with $A = 150$–186. The spin-orbit strength constant $\kappa_{\text{Nils}} = 0.0637$ and quenching factor $q = 0.7$. Exceptions include $V_0^p = 26.5$ MeV, $V_0^n = 22.6$ MeV for Hf and W isotopes, $q = 0.57$ for ^{150}Sm, $r_p^p = 1.57$ fm, $q = 0.78$ for ^{150}Nd, $V_0^p = 23$ MeV, $V_0^n = 20$ MeV, $r_p^p = 2.0$ fm, $r_p^n = 2.4$ fm, $q = 0.5$ for ^{148}Sm and ^{148}Nd, $V_0^p = 26.5$ MeV, $V_0^n = 22.6$ MeV, $r_p^p = 1.7$ fm, $r_p^n = 2.1$ fm, $\kappa_{\text{Nils}} = 0.05$, and $q = 0.57$ for Os and Pt isotopes.

APPENDIX B: EXCITATION PROBABILITIES

Excitation probabilities are calculated with the help of the theory of linear response of the system to a weak external field:

$$\hat{O}(t) = \hat{O}\,e^{-i\Omega t} + \hat{O}^\dagger\,e^{i\Omega t}. \tag{B1}$$

A detailed explanation can be found in [10,11]. We recall only the main points. The matrix elements of the operator $\hat{O}$ obey the relationship [41]

$$|\langle\psi_a|\hat{O}|\psi_0\rangle|^2 = \hbar\lim_{\Omega\to\Omega_a}(\Omega - \Omega_a)\overline{\langle\psi'|\hat{O}|\psi'\rangle e^{-i\Omega t}}, \tag{B2}$$

where ψ_0 and ψ_a are the stationary wave functions of the unperturbed ground and excited states, ψ' is the wave function of the perturbed ground state, and $\Omega_a = (E_a - E_0)/\hbar$ are the normal frequencies, where the bar means averaging over a time interval much larger than $1/\Omega$.

To calculate the magnetic transition probability, it is necessary to excite the system by the following external field:

$$\hat{O}_{\lambda\mu} = \mu_N\left(g_s^\tau\hat{\mathbf{S}}/\hbar - ig_l^\tau\frac{2}{\lambda+1}[\mathbf{r}\times\nabla]\right)\nabla(r^\lambda Y_{\lambda\mu}), \quad \mu_N = \frac{e\hbar}{2mc}. \tag{B3}$$

The free particle g factors are given by $g_l^p = 1$, $g_s^p = 5.5856$ for protons, and $g_l^n = 0$, $g_s^n = -3.8263$ for neutrons. The spin quenching factor q was applied in the calculations: $g_s^\tau = qg_s^{\tau\,\text{free}}$. The values used are given in the text after Eq. (A5). The dipole

operator ($\lambda = 1$, $\mu = 1$) in cyclic coordinates looks like

$$\hat{O}_{11} = \sqrt{\frac{3}{4\pi}} \left[g_s^\tau \hat{S}_1/\hbar - g_l^\tau \sqrt{2} \sum_{\nu,\sigma} C_{1\nu,1\sigma}^{11} r_\nu \nabla_\sigma \right] \mu_N. \tag{B4}$$

For the matrix element we have

$$\langle \psi' | \hat{O}_{11} | \psi' \rangle = \sqrt{\frac{3}{2\pi}} \left[-\frac{\hbar}{2} \left(g_s^n \mathcal{F}^{n\downarrow\uparrow} + g_s^p \mathcal{F}^{p\downarrow\uparrow} \right) - i g_l^p \mathcal{L}_{11}^{p+} \right] \frac{\mu_N}{\hbar} = \sqrt{\frac{3}{8\pi}} \left[\frac{1}{2} \left(g_s^p - g_s^n \right) \bar{\mathcal{F}}^{\downarrow\uparrow} + \frac{i}{\hbar} g_l^p \bar{\mathcal{L}}_{11}^+ + \frac{i}{\hbar} \left[g_s^n + g_s^p - g_l^p \right] \mathcal{L}_{11}^+ \right] \mu_N. \tag{B5}$$

Deriving (B5) we have used the relation $2i\mathcal{L}_{11}^+ = -\hbar \mathcal{F}^{\downarrow\uparrow}$, which follows from the angular momentum conservation [11]. One has to add the external field (B4) to the Hamiltonian (5). Due to the external field some dynamical equations of (A1) become inhomogeneous:

$$\dot{\mathcal{R}}_{21}^+ = \cdots + i \frac{3}{\sqrt{\pi}} \frac{\mu_N}{2\hbar} g_l^p R_{20}^{p+}(\text{eq}) \, e^{i\Omega t},$$

$$\dot{\mathcal{L}}_{11}^- = \cdots + i \sqrt{\frac{3}{\pi}} \frac{\mu_N}{2\hbar} g_l^p L_{10}^{p-}(\text{eq}) \, e^{i\Omega t},$$

$$\dot{\mathcal{L}}_{10}^{\downarrow\uparrow} = \cdots + i \sqrt{\frac{3}{2\pi}} \frac{\mu_N}{2\hbar} \left[g_s^n L_{10}^{n-}(\text{eq}) - g_s^p L_{10}^{p-}(\text{eq}) \right] e^{i\Omega t}. \tag{B6}$$

For the isoscalar set of equations (A2), respectively, we obtain

$$\dot{\mathcal{R}}_{21}^+ = \cdots - i \frac{3}{\sqrt{\pi}} \frac{\mu_N}{2\hbar} g_l^p R_{20}^{p+}(\text{eq}) \, e^{i\Omega t},$$

$$\dot{\mathcal{L}}_{11}^- = \cdots - i \sqrt{\frac{3}{\pi}} \frac{\mu_N}{2\hbar} g_l^p L_{10}^{p-}(\text{eq}) \, e^{i\Omega t},$$

$$\dot{\mathcal{L}}_{10}^{\downarrow\uparrow} = \cdots + i \sqrt{\frac{3}{2\pi}} \frac{\mu_N}{2\hbar} \left[g_s^n L_{10}^{n-}(\text{eq}) + g_s^p L_{10}^{p-}(\text{eq}) \right] e^{i\Omega t}. \tag{B7}$$

Solving the inhomogeneous set of equations one can find the required in (B5) values of $\mathcal{L}_{11}^+$, $\bar{\mathcal{L}}_{11}^+$, and $\bar{\mathcal{F}}^{\downarrow\uparrow}$ and calculate $B(M1)$ factors for all excitations as it is explained in [10,11].

APPENDIX C: CURRENTS

$$\mathcal{L}_{\lambda,\mu}^\varsigma = \int d^3 r \{ r \otimes \delta J^\varsigma \}_{\lambda\mu} = \frac{1}{\sqrt{3}} (-1)^\lambda \left[A_1 C_{1\mu,10}^{\lambda\mu} K_{\mu,0}^\varsigma - A_2 \left(C_{1\mu+1,1-1}^{\lambda\mu} K_{\mu+1,-1}^\varsigma + C_{1\mu-1,11}^{\lambda\mu} K_{\mu-1,1}^\varsigma \right) \right], \tag{C1}$$

$$K_{-1,-1}^\varsigma = -\frac{\sqrt{3} \, \mathcal{L}_{2-2}^\varsigma}{A_2}, \quad K_{-1,0}^\varsigma = \frac{\sqrt{3} \left(\mathcal{L}_{1-1}^\varsigma + \mathcal{L}_{2-1}^\varsigma \right)}{\sqrt{2} A_1}, \quad K_{-1,1}^\varsigma = -\frac{\sqrt{3} \, \mathcal{L}_{10}^\varsigma + \mathcal{L}_{20}^\varsigma + \sqrt{2} \, \mathcal{L}_{00}^\varsigma}{\sqrt{2} A_2},$$

$$K_{0,-1}^\varsigma = \frac{\sqrt{3} \left(\mathcal{L}_{1-1}^\varsigma - \mathcal{L}_{2-1}^\varsigma \right)}{\sqrt{2} A_2}, \quad K_{0,0}^\varsigma = \frac{\sqrt{2} \mathcal{L}_{2,0}^\varsigma - \mathcal{L}_{0,0}^\varsigma}{A_1}, \quad K_{0,1}^\varsigma = -\frac{\sqrt{3} \left(\mathcal{L}_{11}^\varsigma + \mathcal{L}_{21}^\varsigma \right)}{\sqrt{2} A_2},$$

$$K_{1,-1}^\varsigma = \frac{\sqrt{3} \, \mathcal{L}_{10}^\varsigma - \mathcal{L}_{20}^\varsigma - \sqrt{2} \, \mathcal{L}_{00}^\varsigma}{\sqrt{2} A_2}, \quad K_{1,0}^\varsigma = \frac{\sqrt{3} \left(\mathcal{L}_{21}^\varsigma - \mathcal{L}_{11}^\varsigma \right)}{\sqrt{2} A_1}, \quad K_{1,1}^\varsigma = -\frac{\sqrt{3} \, \mathcal{L}_{22}^\varsigma}{A_2}, \tag{C2}$$

where A_i are defined by (A3).

[1] R. R. Hilton, *Lecture Delivered at the International Conference on Nuclear Structure* (Joint Institute for Nuclear Research, Dubna, Russia, 1976) (unpublished).

[2] T. Suzuki and D. J. Rowe, Nucl. Phys. A **289**, 461 (1977).

[3] N. Lo Iudice and F. Palumbo, Phys. Rev. Lett. **41**, 1532 (1978).

[4] E. Lipparini and S. Stringari, Phys. Lett. B **130**, 139 (1983).

[5] S. Stringari, J. Phys. Colloques **45**, C6-265 (1984).

[6] E. B. Balbutsev, L. A. Malov, P. Schuck, M. Urban, and X. Viñas, Phys. At. Nucl. **71**, 1012 (2008).

[7] E. B. Balbutsev and P. Schuck, Ann. Phys. (NY) **322**, 489 (2007).

[8] D. Bohle, A. Richter, W. Steffen, A. E. L. Dieperink, N. Lo Iudice, F. Palumbo, and O. Scholten, Phys. Lett. B **137**, 27 (1984).

[9] K. Heyde, P. von Neumann-Cosel, and A. Richter, Rev. Mod. Phys. **82**, 2365 (2010).

[10] E. B. Balbutsev and P. Schuck, Nucl. Phys. A **720**, 293 (2003); **728**, 471 (2003).

[11] E. B. Balbutsev, I. V. Molodtsova, and P. Schuck, Nucl. Phys. A **872**, 42 (2011).

[12] E. B. Balbutsev, I. V. Molodtsova, and P. Schuck, Phys. Rev. C **91**, 064312 (2015).

[13] E. B. Balbutsev, L. A. Malov, P. Schuck, and M. Urban, Phys. At. Nucl. **72**, 1305 (2009).

[14] V. G. Soloviev, *Theory of Complex Nuclei* (Pergamon, New York, 1976).

[15] P. Ring and P. Schuck, *The Nuclear Many-Body Problem* (Springer-Verlag, Berlin, 1980).

[16] D. A. Varshalovitch, A. N. Moskalev, and V. K. Khersonski, *Quantum Theory of Angular Momentum* (World Scientific, Singapore, 1988).

[17] E. B. Balbutsev, I. V. Molodtsova, and P. Schuck, Phys. Rev. C **97**, 044316 (2018).

[18] V. G. Soloviev, A. V. Sushkov, N. Yu. Shirikova, and N. Lo Iudice, Nucl. Phys. A **600**, 155 (1996).

[19] V. G. Soloviev, A. V. Sushkov, and N. Yu. Shirikova, Phys. Part. Nucl. **31**, 385 (2000).

[20] N. Pietralla, P. von Brentano, R.-D. Herzberg, U. Kneissl, J. Margraf, H. Maser, H. H. Pitz, and A. Zilges, Phys. Rev. C **52**, R2317 (1995).

[21] J. Enders, P. von Neumann-Cosel, C. Rangacharyulu, and A. Richter, Phys. Rev. C **71**, 014306 (2005).

[22] N. Pietralla, P. von Brentano, R.-D. Herzberg, U. Kneissl, N. Lo Iudice, H. Maser, H. H. Pitz, and A. Zilges, Phys. Rev. C **58**, 184 (1998).

[23] T. Renstrøm, H. Utsunomiya, H. T. Nyhus, A. C. Larsen, M. Guttormsen, G. M. Tveten, D. M. Filipescu, I. Gheorghe, S. Goriely, S. Hilaire, Y.-W. Lui, J. E. Midtbø, S. Péru, T. Shima, S. Siem, and O. Tesileanu, Phys. Rev. C **98**, 054310 (2018).

[24] J. Margraf, T. Eckert, M. Rittner, I. Bauske, O. Beck, U. Kneissl, H. Maser, H. H. Pitz, A. Schiller, P. von Brentano, R. Fischer, R.-D. Herzberg, N. Pietralla, A. Zilges, and H. Friedrichs, Phys. Rev. C **52**, 2429 (1995).

[25] T. Otsuka, Nucl. Phys. A **507**, 129c (1990).

[26] A. Kingan, M. Quinonez, X. Yu, and L. Zamik, Int. J. Mod. Phys. E **27**, 1850090 (2018).

[27] S. Valenta, B. Baramsai, T. A. Bredeweg, A. Couture, A. Chyzh, M. Jandel, J. Kroll, M. Krtička, G. E. Mitchell, J. M. O'Donnell, G. Rusev, J. L. Ullmann, and C. L. Walker, Phys. Rev. C **96**, 054315 (2017).

[28] A. S. Adekola, C. T. Angell, S. L. Hammond, A. Hill, C. R. Howell, H. J. Karwowski, J. H. Kelley, and E. Kwan, Phys. Rev. C **83**, 034615 (2011).

[29] R. D. Heil, H. H. Pitz, U. E. P. Berg, U. Kneissl, K. D. Hummel, G. Kilgus, D. Bohle, A. Richter, C. Wesselborg, and P. von Brentano, Nucl. Phys. A **476**, 39 (1988).

[30] J. Margraf, A. Degener, H. Friedrichs, R. D. Heil, A. Jung, U. Kneissl, S. Lindenstruth, H. H. Pitz, H. Schacht, U. Seemann, R. Stock, C. Wesselborg, P. von Brentano, and A. Zilges, Phys. Rev. C **42**, 771 (1990).

[31] S. L. Hammond, A. S. Adekola, C. T. Angell, H. J. Karwowski, E. Kwan, G. Rusev, A. P. Tonchev, W. Tornow, C. R. Howell, and J. H. Kelley, Phys. Rev. C **85**, 044302 (2012).

[32] M. Guttormsen, L. A. Bernstein, A. Bürger, A. Görgen, F. Gunsing, T. W. Hagen, A. C. Larsen, T. Renstrøm, S. Siem, M. Wiedeking, and J. N. Wilson, Phys. Rev. Lett. **109**, 162503 (2012).

[33] V. G. Soloviev, A. V. Sushkov, and N. Yu. Shirikova, Z. Phys. A **358**, 287 (1997).

[34] M. Durand, P. Schuck, and J. Kunz, Nucl. Phys. A **439**, 263 (1985).

[35] P. Schuck and M. Urban, Phys. Rev. C **100**, 031301(R) (2019).

[36] E. B. Balbutsev, I. V. Molodtsova, and P. Schuck, Phys. Rev. C **88**, 014306 (2013).

[37] E. B. Balbutsev, Sov. J. Part. Nucl. **22**, 159 (1991).

[38] F. Palumbo, Phys. Rev. C **99**, 034319 (2019).

[39] N. Lo Iudice, E. Lipparini, S. Stringari, F. Palumbo, and A. Richter, Phys. Lett. B **161**, 18 (1985).

[40] D. Guéry-Odelin and S. Stringari, Phys. Rev. Lett. **83**, 4452 (1999).

[41] A. M. Lane, *Nuclear Theory* (Benjamin, New York, 1964).